JOURNAL OF PETROLOGY | VOLUME 44 | NUMBER 9 | PAGES 1703–1726 | 2003 | DOI: 10.1093/petrology/egg057

Time-scales of Differentiation from Mafic Parents to Rhyolite in North American Continental Arcs

M. K. REAGAN[1]*, K. W. W. SIMS[2], J. ERICH[3], R. B. THOMAS[4], H. CHENG[4], R. L. EDWARDS[4], G. LAYNE[2] AND L. BALL[2]

[1]DEPARTMENT OF GEOSCIENCE, UNIVERSITY OF IOWA, IOWA CITY, IA 52242, USA

[2]DEPARTMENT OF GEOLOGY AND GEOPHYSICS, WOODS HOLE OCEANOGRAPHIC INSTITUTION, WOODS HOLE, MA 02543, USA

[3]EXXON-MOBIL, 800 BELL STREET, HOUSTON, TX 77002, USA

[4]MINNESOTA ISOTOPE LABORATORY, DEPARTMENT OF GEOLOGY AND GEOPHYSICS, UNIVERSITY OF MINNESOTA, MINNEAPOLIS, MN 55455, USA

RECEIVED APRIL 17, 2002; ACCEPTED MARCH 21, 2003

Young rhyolites and associated lavas and magmatic enclaves from the Katmai–Novarupta volcanic system (Alaskan Peninsula), and the Crater Lake and Medicine Lake volcanic system (Cascades) were analyzed for U and Th isotope abundances, as well as major and trace element concentrations, to investigate the time-scales of the processes that lead to rhyolite generation in continental arcs. Basalts and basaltic andesites typically migrate from the mantle to the surface within several thousand years. Variations in $(^{230}Th)/(^{232}Th)$ *and* $(^{238}U)/(^{232}Th)$ *ratios with* SiO_2 *concentrations in intermediate lavas appear to result from crystal fractionation combined with assimilation of recently crystallized magmas. These data also suggest that* $\sim 10^4$–10^5 *years of mafic magmatism are required at a volcanic center to generate silicic andesites and dacites. Rhyolite genesis involves varying proportions of crystal fractionation of intermediate magmas and assimilation of crust. The near-equilibrium* $(^{238}U)/(^{230}Th)$ *ratios for all of the rhyolites suggest an average time since U was last fractionated from Th for the constituents making up these rhyolites of* $>10^5$ *years. Therefore, the residence times of continental magmas and their entrained crystals appear to increase by a minimum of 2–3 orders of magnitude with increasing* SiO_2 *concentrations from basalt to rhyolite.*

KEY WORDS: *time-scales; rhyolite; andesite; Aleutian arc; Cascade arc*

INTRODUCTION

Two seminal overviews of silicic volcanism (Smith, 1979; Hildreth, 1981) led to a significantly clearer understanding of the physical processes leading to rhyolite genesis. Nevertheless, the relative roles of crystal fractionation and crustal melting in generating rhyolites (e.g. Graham *et al.*, 1995), and the lengths of time required to produce and store rhyolitic magmas in the crust (e.g. Davies *et al.*, 1994; Reid *et al.*, 1997; Hawkesworth *et al.*, 2000) are still debated. Studies of migmatites and tonalite–trondhjemite terranes (e.g. Beard, 1995; Thompson & Connolly, 1995), as well as studies of some young volcanic systems (e.g. Halliday *et al.*, 1983; Smith & Leeman, 1987) have shown that some continental silicic magmas can be generated by melting of the crust. In other systems, crystal fractionation of andesitic magmas has been shown to play the dominant role in generating silicic magmas (e.g. Cameron & Hanson, 1982; Bacon & Druitt, 1988). More recent petrological studies have suggested that silicic magmas are produced by a hybrid process of crystal fractionation of mafic magmas combined with assimilation of crustal materials (e.g. Hopson & Mattinson, 1990; Grove *et al.*, 1997).

These different mechanisms of magma generation could result in significantly different crustal residence

*Corresponding author. Telephone: 319-335-1802. Fax: 319-335-1821. E-mail: mark-reagan@uiowa.edu

times for the crystals and melts that make up rhyolite. For example, the rate of rhyolite generation may be slowed during crystal fractionation by a strong flux of heat through the system or by latent heat of crystallization (Hardee & Larson, 1977). In contrast, the rate of rhyolite genesis by crustal anatexis could be rapid if the crust was warm and large amounts of heat and/or water were supplied to it by crystallizing mafic magmas (Huppert & Sparks, 1988). If the mafic magma body was a plexus of dikes, then melting could be particularly rapid (e.g. Bergantz, 1995).

To gain a better understanding of the processes and time-scales required to generate rhyolitic magmas, suites of young cogenetic basaltic to rhyolitic rocks from the Katmai–Novarupta, Crater Lake, and Medicine Lake volcanic systems were analyzed for U and Th isotope abundances, as well as their major and trace element compositions. These volcanic systems span a significant range of erupted volumes, eruptive styles, and geological settings, allowing discrimination of the influence of geological setting on magma generation processes and the time-frames over which they operate.

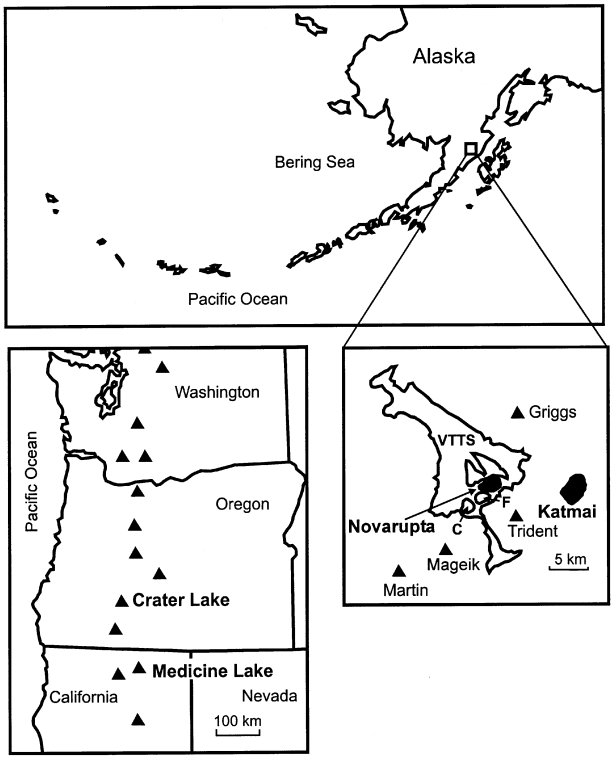

Fig. 1. Location map for the volcanic centers investigated here. The black areas in the expanded view of the Katmai–Novarupta region represent the Novarupta funnel vent and the Katmai caldera. C, Cerberus Dome; F, Falling Mountain Dome; VTTS, Valley of Ten Thousand Smokes.

GEOLOGICAL SETTINGS

Katmai–Novarupta

The Katmai–Novarupta volcanic system is located ~50 km SW of Anchorage on the Alaskan Peninsula. The Novarupta vent is in close proximity to an array of young volcanic edifices (Griggs, Mageik, Martin, Trident, and Katmai) composed of andesite to dacite (Fig. 1). The generation of the 1912 rhyolite has been attributed to this unusual clustering of volcanoes in the Aleutian arc and the associated crustal heating (Hildreth, 1983). The oldest recorded local volcanism was at Mount Griggs at 292 ka (Hildreth & Fierstein, 2000). The Cerberus and Falling Mountain dacite domes were emplaced during the Pleistocene (Hildreth & Fierstein, 2000). The youngest volcanism occurred on the SW flank of Mount Trident between 1953 and 1974 (Coombs *et al.*, 2000).

The explosive eruption of 1912 from Novarupta first ejected a high-silica rhyolite, followed by dacite with minor rhyolite, then andesite plus dacite with minor rhyolite (Hildreth, 1983, 1987). The eruption concluded with the extrusion of a small dacitic dome in the caldera formed by the collapse of Mount Katmai, and the Novarupta rhyolite dome (Hildreth & Fierstein, 2000).

Magmas erupted in 1912 are separated by a compositional gap. Rhyolite averaging 77·0 ± 0·6 wt % SiO_2 accounts for about 7–8 km^3 of the ~13 km^3 of magma that erupted. Approximately 5·5 km^3 of dacite and andesite with 58·5–66 wt % SiO_2 also erupted (Hildreth, 1987; Hildreth & Fierstein, 2000). Variations in $\delta^{18}O$ and $^{87}Sr/^{86}Sr$ isotopic compositions, incompatible trace element concentrations, magmatic temperatures, and experimentally determined pressures of phase equilibria (Coombs & Gardner, 2001) suggest that all of the 1912 ejecta were compositionally and physically linked (Hildreth, 1983). Conversely, the distinct compositional gap between the dacites and rhyolites has been interpreted to indicate that silicic magmas from deep within the crust intermingled with shallower intermediate magmas before erupting in 1912 (Eichelberger *et al.*, 2000).

Crater Lake

Crater Lake lies on the axis of the Cascade volcanic arc in Oregon (Fig. 1), and is one of its major volcanic centers. The Crater Lake caldera formed during the climactic eruption of Mount Mazama at 7·7 ka. The oldest Mazama lava is an ~420 ka andesite flow (Bacon, 1983). Significant dacitic volcanism occurred between ~70 and 40 ka and a major andesite eruption occurred at ~43 ka. Subsequent flows erupted over

a wide area encompassing the region of the present caldera, indicating the development of a large magma chamber (Bacon, 1983, 1985). Pre-climactic rhyodacite flows erupted in three groups (Bacon & Druitt, 1988). The first two groups erupted between 30 and 13 ka (Bacon, 1983). The third group is close in age and composition to the climactic eruption of 6845 ± 45 radiocarbon years BP (7·7 ka in calendar years, Bacon *et al.*, 2000). This group includes the Lao Rock eruptive sequence at 7015 ± 45 radiocarbon years BP, and the Cleetwood flow, which was still hot when the climactic eruption began (Bacon, 1983; Bacon & Druitt, 1988). The climactic eruption of Mount Mazama itself began with a Plinian ejection of rhyodacitic pumice, which produced an air-fall deposit followed by rhyodacite pyroclastic flows forming the Wineglass Welded Tuff. Crystal-rich andesite and basalt (48–61% SiO_2) were ejected near the end of the climactic eruption, and partially melted granitoid blocks were ejected as the eruption came to a close. The total volume of material ejected was ~47 km^3 (Bacon, 1983).

Andesites from the climactic eruption have been divided into two groups distinguished by their concentrations of Sr and other incompatible trace elements (Bacon & Druitt, 1988; Druitt & Bacon, 1989). These andesites also have distinct isotopic compositions. Low-Sr andesites have relatively low concentrations of incompatible trace elements and $^{87}Sr/^{86}Sr$ = 0·7036–0·7038, whereas nearly all high-Sr andesites are enriched in incompatible trace elements and have $^{87}Sr/^{86}Sr = 0·7033–0·7035$ (Bacon *et al.*, 1994). A broad compositional gap separates these andesites from climactic rhyodacite, which has $SiO_2 = 70·4 \pm 0·3$ wt % (Bacon & Druitt, 1988). The concentrations of most incompatible trace elements in the climactic rhyodacite and in the older rhyodacites generally overlap (Bacon & Druitt, 1988). In contrast, the Sr isotopic compositions of the climactic rhyodacites range from 0·70354 to 0·70358, which is less radiogenic than those of the older rhyodacites (0·7036–0·7038; Bacon *et al.*, 1994), consistent with the climactic rhyodacite consisting of a mixture of older rhyodacite magma produced by differentiation of low-Sr andesite and younger rhyodacite magma produced by differentiation of high-Sr andesite. Thus, Bacon & Druitt (1988) concluded that the climactic low-Sr andesites had longer residence times in the crust than the high-Sr andesites, and the climactic rhyodacite developed over the entire period of this andesitic magmatism.

Medicine Lake

Medicine Lake is a Pleistocene to Holocene shield volcano lying ~45 km east of the Cascades volcanic front at the western margin of the Basin and Range tectonic province (Fig. 1). The Medicine Lake volcano was built over the past 500–600 kyr (Donnelly-Nolan, 1998) by compositionally diverse lavas, ranging from low-K basalts to relatively incompatible element enriched andesites and rhyolites (Mertzman, 1977, 1979; Mertzman & Williams, 1981; Grove *et al.*, 1982, 1988; Grove & Donnelly-Nolan, 1986; Donnelly-Nolan *et al.*, 1990).

Medicine Lake volcano has had a rich Holocene eruptive history (Donnelly-Nolan *et al.*, 1990). Giant Crater produced a large volume eruption of basalt at ~12·7 ka (Baker *et al.*, 1991; Donnelly-Nolan *et al.*, 1991). The Pit Crater silicic andesite erupted at ~4·9 ka, and the basalts of Black Crater and Ross Chimneys erupted at ~3·2 ka. The andesitic Burnt Lava flow (Grove *et al.*, 1988) erupted at ~2·8 ka, followed by the Medicine dacite and Hoffman rhyolite flows. The basalts and andesites making up the Callahan flow erupted at ~1·0 ka. The Little Glass Mountain and Crater Glass rhyolitic eruptions occurred shortly thereafter (Heiken, 1978; Donnelly-Nolan *et al.*, 1990).

The most recent eruption of the Medicine Lake volcano occurred at Glass Mountain. It began with ejection of rhyolite tephra from a chain of vents stretching NW from the Glass Mountain vent. This was followed by effusion of the Glass Mountain dacite, which is noteworthy in the abundance of quenched andesite enclaves with diameters as large as 0·5 m (e.g. Eichelberger, 1981). This flow was dated at 885 radiocarbon years BP (~800 calendar years BP; Donnelly-Nolan *et al.*, 1990). Enclave-poor rhyolite flows and domes erupted from the summit of Glass Mountain after the dacite. The eruption concluded with the extrusion of the rhyolite dome that constructs the Glass Mountain summit. The total volume erupted was ~1 km^3 (Donnelly-Nolan *et al.*, 1990).

The magmatic inclusions found in the Glass Mountain lavas have compositions ranging from basalt to silicic andesite; these include quenched enclaves as well as hornblende- and olivine-gabbro cumulate enclaves (Grove *et al.*, 1997). The cumulate gabbros consist of relatively coarse-grained plagioclase, augite, olivine, orthopyroxene, Fe–Ti oxides, ± amphibole together with accessory apatite and more rarely zircon. Crystalline phases are typically set in vesicular glass, which may contain microlites (Mertzman & Williams, 1981; Grove & Donnelly-Nolan, 1986). Quenched enclaves are characterized by crenulated and sometimes chilled margins, and skeletal to acicular mineral phases set in a matrix of vesicular silicic glass (Eichelberger, 1981; Grove & Donnelly-Nolan, 1986; Grove *et al.*, 1997). The composition of the Glass Mountain dacite has been explained by mixing

magma similar to that of the quenched andesite enclaves with the Glass Mountain rhyolite. Therefore, it appears that the enclave-producing andesite both mixed and mingled with the rhyolite before eruption (e.g. Eichelberger, 1981; Grove *et al*., 1997).

SAMPLES

Katmai–Novarupta

Pumice and scoria blocks from the 1912 pyroclastic deposits collected for this project include a silicic andesite (K90And), a dacite (K90Dac), and a high-silica rhyolite (K90Rhy; Table 1). Samples from the Mount Cerberus (K90CB) and Falling Mountain (K90FM) domes, the 1912 Novarupta dome (K90Nov), and a lava erupted in 1961 from Trident (K90TR) were also collected. E. W. Hildreth contributed a basaltic andesite clast (K851) from the 1912 eruption tephra deposits and a low-silica rhyolite (K2043) from the interior wall of the Katmai caldera with an age of 22 ka (Hildreth & Fierstein, 2000).

All of the andesites and dacites are coarsely porphyritic with phenocrysts of plagioclase, augite, orthopyroxene, and Fe–Ti oxides. Apatite is also present in the silicic andesites and dacites. About 0·5–1% anhedral olivine is present in K90TR, and is present in lower proportions in most of the other intermediate composition samples. These olivine crystals generally are rimmed by orthopyroxene microlites. Glomeroporphyritic clots of plagioclase, orthopyroxene, clinopyroxene, and Fe–Ti oxides with textures ranging from gabbroic to fine grained and acicular are present in many samples. These clots are particularly abundant in the 1912 samples. Rare euhedral hornblende crystals are present in the silicic andesites and dacites erupted in 1912. The major phenocrysts exhibit complex zoning profiles, varying crystal morphologies, and diverse inclusion populations, reflecting complex polybaric crystallization and mixing (e.g. Coombs *et al*., 2000). Severe post-eruption oxidation partially to completely replaced pyroxenes by opaque minerals in the Cerberus and Falling Mountain dacites.

The 1912 rhyolite pumice from Novarupta (e.g. K90Rhy) has ~1% weakly zoned plagioclase phenocrysts that are <1 mm in length (Hildreth & Fierstein, 2000). The Novarupta dome rhyolite (e.g. K90Nov) has ~3% phenocrysts including plagioclase similar to that found in the rhyolitic pumice, together with inclusion-rich plagioclase, augite, hornblende and opaques.

Crater Lake

All of the studied samples from Crater Lake were collected by C. R. Bacon from large single pumice or scoria blocks ejected during the climactic eruption. The rhyodacite (88c:1533) has a SiO_2 concentration of 70·2 wt % (volatile-free; see Table 1), which is typical for the climactic rhyodacites (Bacon & Druitt, 1988). It is sparsely porphyritic with ~10 vol. % crystals of euhedral to anhedral plagioclase and minor amounts of orthopyroxene, augite, opaques, and apatite (see also Druitt & Bacon, 1989).

Both andesite scoria samples (low-Sr, 88c:1532; high-Sr, 88c:1534) are characterized by high crystal contents (88c:1532 ~60 vol. %; 88c:1534 ~50 vol. %) of plagioclase, orthopyroxene, clinopyroxene, hornblende, Fe–Ti oxides, and apatite (see also Druitt & Bacon, 1989). The low-Sr andesite has euhedral to subhedral plagioclase crystals up to 5 mm in length. These crystals have large glass and vapor-filled inclusions, and exhibit complex zoning patterns that appear to represent multiple sequences of growth and resorption. The pyroxenes are euhedral to anhedral and <1 mm in length. Hornblende is less abundant and generally more euhedral than the pyroxenes. Crystals of hornblende are up to 3 mm in length, have relatively low aspect ratios, and commonly contain inclusions of the other phenocryst phases.

Hornblende is the dominant mafic mineral in the high-Sr andesite (88c:1534). It is euhedral to subhedral, has a high aspect ratio, and commonly has large glass and vapor-filled inclusions, consistent with rapid cooling and a single pulse of crystal growth. Plagioclase morphologies range from euhedral to anhedral. Some euhedral crystals lack glass inclusions and either can have relatively homogeneous cores, or can be strongly zoned from core to rim. Some crystals have abundant glass inclusions. Anhedral plagioclase crystals with textural evidence of multiple melting and growth events are less common than in the low-Sr andesite.

Medicine Lake

J. M. Donnelly-Nolan contributed the samples from Medicine Lake volcano. Sample 82-72f was collected from one of the youngest Giant Crater lavas. It is relatively primitive with 10·6 wt % MgO and 47·6 wt % SiO_2, and it lacks large phenocrysts (Baker *et al*., 1991; Donnelly-Nolan *et al*., 1991). The samples of the Black Crater (733 m) and Callahan (1513 m) lavas are differentiated calcalkaline basalts with 50·1 wt % SiO_2 and 51·4 SiO_2, respectively (Table 1). Callahan basalts are sparsely porphyritic with rare crystals of olivine and plagioclase (Kinzler *et al*., 2000), In contrast, Black Crater basalts are coarsely porphyritic with ~25% plagioclase and 2–4% olivine (Sisson *et al*., 1990). The Burnt Lava flow andesite (695 m) has ~4% crystals of plagioclase, olivine,

Table 1: Major and trace element compositions of representative whole rocks

	Crater Lake[1]			Katmai–Novarupta[1]								
Sample:	88c:1532	88c:1533	88c:1534	K90Rhy	K90Nov	K90Dac	K90And	K851[2]	K2043[2]	K90CB	K90FM	K90TR
Age:	7·7 ka	7·7 ka	7·7 ka	AD 1912	AD 1912	AD 1912	AD 1912	AD 1912	22·5 ka	L. Pleist.	L. Pleist.	1959
SiO_2	55·10	68·10	55·50	75·49	73·77	64·52	61·83	54·63	71·70	64·40	64·76	61·25
TiO_2	1·01	0·47	1·03	0·15	0·23	0·68	0·68	0·77	0·40	0·63	0·61	0·73
Al_2O_3	19·00	14·60	18·60	12·13	14·35	15·45	16·37	17·05	14·51	16·13	16·18	16·63
Fe_2O_3*	8·06	2·62	7·24	0·87	1·72	6·02	6·22	8·24	2·81	5·99	5·47	6·65
MnO	0·12	0·05	0·08	0·03	0·05	0·12	0·11	0·14	0·07	0·11	0·11	0·12
MgO	3·87	0·83	3·37	0·08	0·28	2·05	2·60	5·39	0·71	2·42	2·07	3·14
CaO	7·89	2·23	7·79	0·77	1·06	4·79	5·97	9·44	2·72	5·51	5·17	6·74
Na_2O	3·98	4·98	4·25	3·36	4·56	4·17	3·71	2·94	4·42	3·95	4·09	3·89
K_2O	0·71	2·48	1·03	3·09	3·37	1·71	1·56	0·87	2·39	1·51	1·58	1·37
P_2O_5	0·32	0·11	0·43	0·01	0·04	0·14	0·13	0·13	0·12	0·11	0·13	0·14
Total	100·06	96·47	99·32	95·97	99·43	99·64	99·19	99·60	99·85	100·77	100·17	100·66
LOI	0·42	2·97	0·45	3·45	1·10	0·91	0·90		0·59	0·00	0·00	–0·09
Li					31·52							
Be					1·59							
Cs	0·73	2·84	0·82	2·45	2·33	1·28	1·30			0·93	0·92	1·04
Rb	12·8	49·6	16·0	63·1	63·6	34·3	33·5			29·4	29·0	26·4
Ba	257	696	349	976	947	562	529			527	531	450
Sr	772	373	1387	65	75	252	283			283	304	320
Pb	3·94	7·61	5·39	13·25	13·29	7·32	7·59			5·53	5·31	6·05
Th	1·11	4·95	2·11	5·57	5·54	3·11	3·50			2·65	2·37	2·63
U	0·55	2·20	0·79	2·60	2·57	1·44	1·56			1·13	1·05	1·19
Nb	2·00	6·27	3·15	5·43	5·19	3·97	3·81			3·21	3·23	3·26
Ta	0·14	0·42	0·19	0·41	0·42	0·27	0·25			0·22	0·23	0·22
Zr	65·2	240·4	105·9	183·3	178·7	161·1	160·8			107·7	82·5	133·3
Hf	1·67	6·15	2·81	5·68	5·58	4·26	4·36			3·11	2·65	3·67
La	7·11	19·33	15·14	18·49	18·40	11·93	11·75			10·30	10·95	10·14
Ce	14·97	40·99	35·33	39·61	40·74	26·32	25·85			22·43	24·16	22·23
Pr	2·23	5·25	5·03	5·56	5·59	3·83	3·79			3·26	3·49	3·33
Nd	10·04	21·01	21·93	23·99	23·85	17·22	16·83			14·52	15·33	15·19
Sm	2·38	4·15	4·22	5·81	5·78	4·33	4·15			3·62	3·71	3·82
Eu	0·96	1·05	1·41	0·88	1·02	1·16	1·16			1·04	1·08	1·12
Gd	2·45	3·97	3·75	6·29	6·30	4·81	4·60			4·00	4·08	4·33
Tb	0·41	0·68	0·59	1·18	1·10	0·88	0·84			0·73	0·73	0·78
Dy	2·16	3·71	2·99	7·00	6·84	5·12	4·84			4·21	4·17	4·53
Ho	0·44	0·76	0·56	1·56	1·51	1·13	1·06			0·92	0·89	0·99
Er	1·17	2·18	1·48	4·50	4·43	3·19	3·00			2·63	2·52	2·80
Yb	1·08	2·23	1·26	4·76	4·67	3·34	3·11			2·70	2·50	2·89
Lu	0·17	0·36	0·19	0·78	0·75	0·54	0·51			0·43	0·39	0·46
Y	12·6	22·2	15·7	45·8	45·0	33·4	30·2			27·1	25·2	28·1
V	214·6	32·5	168·6	2·3	7·9	125·8	142·8			131·9	122·6	179·2
Sc	18·2	6·6	15·6	7·5	8·2	17·9	20·8			18·7	16·3	23·4
Ni	42·3	3·2	25·2	1·3	2·5	7·2	6·1			6·1	5·2	11·8
Cr	37·1	3·5	23·6	1·6	1·3	21·4	23·7			21·4	7·7	41·8
Co	26·5	3·2	21·6	0·6	1·0	12·2	14·8			14·6	12·5	18·2
Cu	41·0	9·1	75·8	6·1	3·8	29·4	16·5			21·4	19·3	31·0
Zn	78·5	29·1	67·8	30·5	35·3	69·0	30·5			61·8	60·8	71·1
Ga	19·96	16·90	20·84	12·80	11·05	16·53	16·75			16·52	15·98	17·09

Table 1: continued

	Medicine Lake[3]											Standards[3]	
Sample:	1368 m	1331 m[4]	1413 m[5]	945 m	1139 ma	1424 ma	1545 m	695 m[6]	1513 m	733 m	82–72f	JR-1	MAS1722
Age:	800 BP	800 BP	800 BP	4·9 ka	800 BP	800 BP	800 BP	2·8 ka	1000 BP	3·2 ka	12·7 ka		
SiO_2	71·79	73·00	63·30	62·45	54·12	57·22	57·65	56·50	51·43	50·09	47·59	76·80	49·81
TiO_2	0·36	0·28	0·63	0·83	0·91	0·76	0·75	0·64	0·94	0·81	0·57	0·10	1·08
Al_2O_3	14·25	13·70	16·10	16·27	17·88	17·19	17·30	16·50	17·74	17·91	18·30	13·17	15·15
Fe_2O_3*	2·42	1·93	5·13	5·58	8·31	6·90	6·97	6·69	9·27	8·81	9·04	0·89	13·27
MnO	0·04	0·03	0·08	0·09	0·12	0·11	0·10	0·11	0·14	0·14	0·13	0·10	0·20
MgO	0·51	0·36	2·93	2·43	5·64	5·12	4·70	5·78	6·80	8·37	10·62	0·13	5·32
CaO	1·76	1·32	5·13	5·21	9·03	7·37	7·57	7·99	9·72	10·82	11·71	0·76	10·06
Na_2O	4·28	3·95	3·80	3·77	3·38	3·48	3·61	3·07	3·28	2·72	2·22	4·01	2·79
K_2O	3·82	4·29	2·50	2·44	0·85	1·47	1·45	1·62	0·55	0·45	0·07	4·67	1·07
P_2O_5	0·07	<0·05	0·14	0·22	0·17	0·14	0·15	0·10	0·17	0·11	0·05	0·02	0·26
Total	99·30	98·86	99·74	99·28	100·41	99·74	100·25	99·00	100·05	100·23	100·32	100·65	99·01
LOI	0·91	0·42	0·04	0·27	−0·04	0·29	0·00		−0·35	−0·27	−0·23		
Li	51·51			38·67	17·09	21·76	22·09		8·84	8·09	2·52	60·54	10·94
Be	2·56			2·03	0·978	1·23	1·31		0·781	0·619	0·209	3·79	1·01
Cs	8·68	9·5		4·59	1·11	2·50	2·56	3·52	0·52	0·81	0·09	19·94	0·90
Rb	131·2	129	86	85·2	23·6	44·4	46·3	51	11·2	13·2	2·1		23·6
Ba	775	796	602	650	285	382	400	329	203	120	23·2	47	871
Sr	134	114	318	358	452	422	424	198	376	222	175	28	439
Pb	17·35			12·92	4·64	7·15	7·50		2·84	2·13		19·68	4·06
Th	12·82	14·3	7·8	7·88	2·14	4·16	4·30	5·4	1·03	1·27	0·18	26·66	1·83
U	4·83	5·1		2·48	0·72	1·46	1·51		0·39	0·49	0·07	8·59	1·46
Nb	9·25	9	10	9·10	4·62	5·18	5·49	3	3·90	3·36	0·64	15·95	2·97
Ta	0·90			0·73	0·32	0·40	0·42	0·45	0·25	0·25	0·06	1·74	0·19
Zr	239·0	216	185	197·4	110·9	129·2	137·5	122	104·5	91·0	39·1	104·5	107·2
Hf	5·95	5·8		4·63	2·58	3·10	3·22	3·00	2·43	2·07	0·96	4·87	2·77
La	21·81	22·9	17·6	21·26	10·04	12·25	12·89	11·2	7·30	4·98	1·35	19·74	10·87
Ce	43·59	43·5	33·6	44·75	22·51	26·35	27·77	22·2	17·52	12·29	4·10	46·94	23·72
Pr	5·09			5·51	2·94	3·28	3·46		2·41	1·73	0·66	5·99	3·49
Nd	18·86	18	16·4	22·00	12·84	13·63	14·30	12·8	11·21	8·30	3·61	23·39	16·31
Sm	3·93	4·1	3·83	4·75	3·13	3·12	3·28	3·06	3·00	2·41	1·31	5·71	4·21
Eu	0·82	0·59	0·85	1·19	1·04	0·94	0·98	0·74	1·04	0·88	0·57	0·27	1·42
Gd	3·78			4·52	3·36	3·21	3·39		3·50	3·14	1·94	5·85	4·52
Tb	0·65	0·66	0·53	0·73	0·57	0·54	0·56	0·55	0·61	0·57	0·37	1·04	0·74
Dy	3·80			4·07	3·32	3·14	3·30		3·79	3·71	2·47	6·37	4·46
Ho	0·79			0·81	0·69	0·65	0·68		0·83	0·84	0·58	1·37	0·94
Er	2·30			2·21	1·93	1·82	1·89		2·35	2·46	1·66	4·07	2·63
Yb	2·51	2·52	2·26	2·16	1·90	1·81	1·87	2·44	2·33	2·57	1·74	4·60	2·55
Lu	0·40	0·36	0·32	0·33	0·29	0·28	0·30	0·37	0·37	0·40	0·27	0·74	0·41
Y	24·2	27	31	23·0	19·3	18·5	19·4	21	23·1	24·3	16·6	43·8	26·5
V	23·2			119·0	197·3	147·9	149·9		202·5	185·3	183·1		396·8
Sc	6·1	4·6		15·9	26·5	20·6	20·6	25·7	30·1	35·3	32·6	5·3	38·7
Ni	1·6		55	13·7	47·1	72·3	64·9	90	75·1	111·3	221·9	−0·2	24·5
Cr	1·9	1·6		13·6	85·3	65·1	62·4	98	102·7	124·6	163·6	1·0	38·9
Co	3·5	2·2		15·3	29·5	24·9	24·0	49	34·2	39·0	45·9		

	Medicine Lake[3]											Standards[3]	
Sample:	1368 m	1331 m[4]	1413 m[5]	945 m	1139 ma	1424 ma	1545 m	695 m[6]	1513 m	733 m	82–72f	JR-1	MAS1722
Age:	800 BP	800 BP	800 BP	4·9 ka	800 BP	800 BP	800 BP	2·8 ka	1000 BP	3·2 ka	12·7 ka		
Cu	12·1			33·3	45·2	45·2	62·2		68·8	91·2	127·7		
As	3·12			0·92	0·61	0·99	1·14		0·60	0·68	0·20		
Ga	15·95			18·96	17·48	17·29	17·98		16·72	13·90	12·65	15·60	17·61

*Total Fe as Fe_2O_3.
[1]Analyzed at the University of Kansas.
[2]Data from Wes Hildreth.
[3]Analyzed at Boston University.
[4]Data from the USGS Analytical Chemistry Services and Julie Donnelly-Nolan.
[5]From Grove *et al*. (1997)
[6]From Grove *et al*. (1988).

orthopyroxene, clinopyroxene, Fe–Ti oxides, and quartz with complex morphologies and zoning patterns (Grove *et al*., 1988). The Pit Crater andesite (945 m) has 62·9 wt % SiO_2 (volatile-free) with rare microphenocrysts of plagioclase, pyroxenes, and Fe–Ti oxides (J. M. Donnelly-Nolan, personal communication, 1991).

Samples from the Glass Mountain eruptives were chosen to span its compositional range and include an early 72·3% SiO_2 (volatile-free) rhyolite bomb (1368 m), a 63·5 wt % SiO_2 dacite (1413 m), and a late 73·8 wt % SiO_2 dome rhyolite (1331 m; Table 1). The rhyolites are sparsely porphyritic with $<1\%$ euhedral to subhedral phenocrysts of plagioclase, orthopyroxene, clinopyroxene, and Fe–Ti oxide. Dacite sample 1413 m has $\sim5\%$ of the same phenocryst assemblage, mostly with subhedral to anhedral morphologies. It also contains $\sim5\%$ quenched andesitic enclaves with sizes ranging from 0·1 to 2 mm.

Magmatic inclusions from Glass Mountain analyzed here include an amphibole-bearing gabbro (1139ma) from the Glass Mountain rhyolite (see Grove *et al*., 1997) and quenched textured andesites (1545 m and 1424 ma) from the Glass Mountain dacite. The gabbro has coarse interlocking crystals of plagioclase, augite, orthopyroxene, hornblende, olivine, and Fe–Ti oxides. Reaction assemblages are present with remnant olivine surrounded by orthopyroxene and remnant augite surrounded by hornblende. Glass, vesicles, and microlites of plagioclase, pyroxenes, hornblende, and opaques fill the spaces between these grains. The largest crystals in the quench-textured andesites are olivine and augite. These are embedded in a matrix of finely intergrown olivine, plagioclase, pyroxene, Fe–Ti oxides, and glass. Sample 1545 m also has scattered large anhedral plagioclase crystals (see Eichelberger, 1981; Grove *et al*., 1997).

ANALYTICAL METHODS

Sample processing

Whole-rock samples were broken into <3 cm fragments, washed in deionized water, dried, crushed, and randomized. A portion of the crushed sample was ground to a fine powder in an alumina shatterbox; another portion was comminuted in a steel disk grinder and sieved. Silicate minerals were separated from the 80–120 or 120–170 sieve fractions using standard density and magnetic techniques. A portion of the 80–120 fraction was ground in an agate mortar with acetone for separation of magnetite using a hand magnet.

Major and trace elements

Major elements (SiO_2, Al_2O_3, TiO_2, Fe_2O_3, MnO, CaO, MgO, Na_2O, K_2O, P_2O_5) were analyzed by inductively coupled plasma emission spectrometry (ICPES) in laboratories under the guidance of Terry Plank at the University of Kansas and Boston University. Both laboratories utilized similar analytical techniques and Jobin–Yvon instruments. Samples were first ignited at 950°C for 30–45 min, then mixed with a lithium metaborate flux (100 mg sample to 400 mg flux), and fused at 1050°C for 15 min. Molten beads were poured into 50 ml of 5% HNO_3 and agitated until dissolved. Solutions were then filtered and diluted to $\sim$4500 times the original ignited powder weight. Four rock standards and a blank were prepared with each batch of 10 unknown samples. Sample solutions were then analyzed, interspersed with standards, drift monitoring solutions, and blanks. RSDs of replicates are generally $<4\%$.

Trace elements were analyzed at the same institutions using similar inductively coupled plasma mass spectrometry (ICPMS) techniques. Samples were

dissolved in a $HF–HNO_3$ mixture (50 mg of powder to 1 ml 18N HF and 3 ml 8N HNO_3), dried, taken up in a HNO_3 solution, and diluted by weight to 1:1500–2000 in parallel with a set of four rock standards and a blank. The samples were then analyzed with the standards, blanks, and a drift monitoring solution on a VG PlasmaQuad ExCell (Boston University) or Fisons/VG PlasmaQuad IIXS (University of Kansas). Routine precision is 1–2% RSD for most trace element to <20 ppb in the rock (see Kelley *et al.*, 2003).

U, Th, and Pb isotopes

Before analyzing for U and Th concentrations and isotopic compositions, silicate mineral separates were inspected under a binocular microscope to remove any obvious inclusions. They were then ultrasonically washed with 0·5N HCl + 2% H_2O_2 solution for 30 min. The supernate was decanted off and the minerals were rinsed several times with water. Finally, the separates were dried, allowed to cool to room temperature, and weighed again to account for potential loss of mass during the cleaning process. These separates as well as whole-rock powders were dissolved in a $HF–HNO_3–HClO_4$ mixture. Magnetite separates were dissolved in $HCl–HNO_3–HF–HClO_4$ mixture.

U and Th isotope measurements at the Minnesota Isotope Laboratory (MIL) used thermal ionization mass spectrometry and chemical separation methods discussed by Edwards *et al.* (1987), Asmerom & Edwards (1995), and Cheng *et al.* (2000). In short, samples were taken completely into solution in 6N HCl and dried. Large aliquots of this solution ($\sim$90%) were used to analyze for ^{230}Th and U concentrations as well as U isotopic compositions. A smaller aliquot ($\sim$10%) was used to analyze for ^{232}Th concentrations. Appropriate amounts of ^{229}Th spike were added to both solutions. A mixed $^{233}U–^{236}U$ spike was added to the large aliquot. Both solutions were refluxed for several hours, fumed, and dried after adding $HClO_4$. U and Th in silicate mineral separates were preconcentrated using Fe-coprecipitation. All samples were taken up in HNO_3, and run through anion exchange columns to separate and purify U and Th. Mass spectrometry was performed on a Finnigan MAT 262 thermal ionization mass spectrometer with a retarding potential quadrupole energy filter (RPQ). U and Th isotopes were analyzed using a multiplier with the RPQ. U isotope ratios were adjusted using the $^{233}U/^{236}U$ ratio of the spike to correct for mass bias. All samples were loaded on triple zone refined rhenium filaments. U was loaded as a nitrate using a double filament arrangement. Th typically was loaded on single filaments with graphite, although a few samples were loaded as a fluoride in a double filament arrangement. Typical procedural blanks were 0·1–0·02 pmol for U and 0·01–0·03 pmol for Th. Listed errors (2σ) are total analytical errors excluding uncertainties in decay constants.

U and Th analyses at Woods Hole Oceanographic Institute (WHOI) employed chemical and mass-spectrometry techniques discussed in detail by Goldstein *et al.* (1989) and Layne & Sims (2000). Sample dissolution techniques were similar to those employed at MIL. However, at WHOI, large aliquots were used to determine the U and Th isotopic compositions (IC). Small aliquots were used to determine U and Th concentrations by isotope dilution (ID). The latter were spiked with ^{229}U and ^{233}U solutions before refluxing for several hours, fuming with perchloric acid, drying, and purification using a single anion exchange column procedure that did not separate U from Th. U and Th were extracted from the large aliquot, separated from each other, and purified using standard anion exchange techniques. The purified Th fractions were loaded onto a polished graphite disk, and their $^{230}Th/^{232}Th$ ratios were determined using a Cameca IMS 1270 secondary ion mass spectrometer (see Layne & Sims, 2000). U isotopic compositions and U and Th concentrations were measured by ICPMS on a Finnigan MAT Element system. NBS 960 was run between each analysis in both the ID and IC runs to monitor mass bias. Procedural blanks for Th and U were 0·25 and 0·05 pmol, respectively. The total analytical errors (2σ) listed in Table 3 (below) are based on triplicate analyses. These errors for U and Th concentrations are $\sim$0·7%, and 0·6% for $^{234}U/^{238}U$ ratios.

Pb was separated from sample solutions and purified using a single anion exchange column with 0·2 ml of resin. The Pb was fixed to the column using 0·5N HBr and was washed off with 0·2N HCl. The Pb was analyzed by ICPMS using the Finnigan MAT Neptune multicollector system at WHOI, with a Tl spike to correct for mass fractionation. All data were normalized to NBS 981 (Todt *et al.*, 1996). The measured procedural blank was 1·5 pmol, with an isotopic composition equal to NBS 981, suggesting that this blank was a carryover from the preceding runs of NBS 981.

GENERAL GEOCHEMISTRY

Mafic and intermediate rocks

The Giant Crater basalt (82-72f) from the Medicine Lake volcano is a relatively primitive high-Al olivine tholeiite with a light REE (LREE)-depleted pattern and relatively low concentrations of K and other highly incompatible elements (Donnelly-Nolan *et al.*, 1991). In contrast, the Black Crater (733) and Callahan basalts (1513 m) are more enriched in LREE

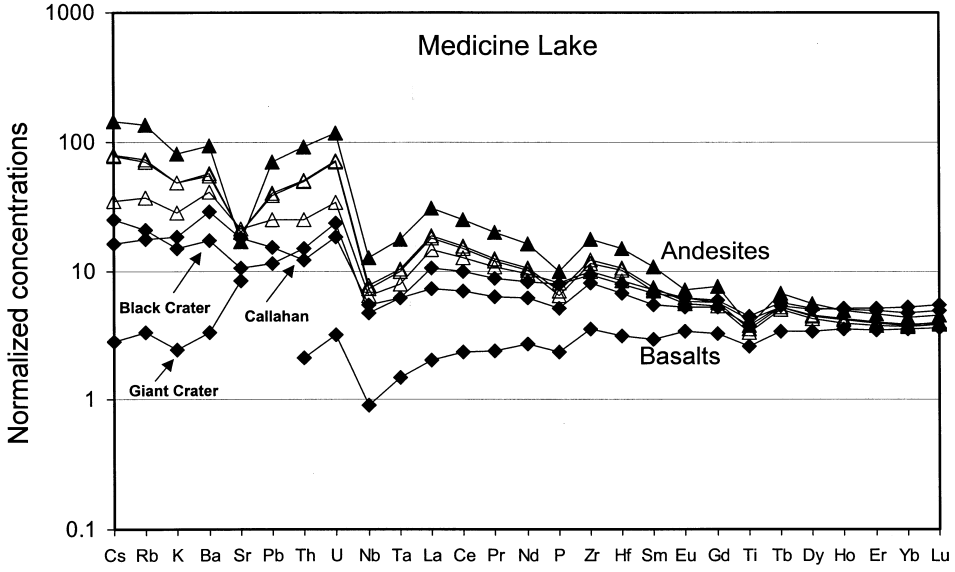

Fig. 2. Normalized incompatible trace element concentrations for basalts and andesites from the Medicine Lake volcano. Data are from Table 1. ▲, andesitic lavas; △, andesite enclaves; ◆, basalts. Elements are arranged by group and degree of incompatibility. Elements considered to have high concentrations in fluids from subducting lithosphere (large-ion lithophile elements and the U-group elements U, Th, and Pb) are to the left. Less soluble REE and high-field strength elements are to the right. Incompatibility during melting generally decreases to the right. Sample concentrations are normalized to the primitive mantle compositions of Sun & McDonough (1989).

and highly incompatible elements (Table 1; Fig. 2). Glass inclusions of low-K tholeiite in olivine from a Black Crater basalt have been shown to have very low water contents (<0·2 wt %; Sisson & Grove, 1993), whereas Callahan basalts apparently had significantly higher water contents during crystallization (3–6 wt %; Kinzler *et al.*, 2000). The Callahan basalt analyzed here also has relatively high Ba/La ratios compared with the low-K Giant Crater basalt. Nevertheless, the Ba/La ratios are generally lower in all Medicine Lake basalts than they are in most of the samples from the other volcanic centers studied here. Thus, its behind-the-volcanic-front setting may have resulted in a lower proportion of subducted constituents in the Medicine Lake lavas compared with those of the other centers.

Incompatible trace element abundances for andesitic lavas and magmatic enclaves from the Medicine Lake volcano are marked by relatively constant heavy REE (HREE) contents, but La/Sm and Th/La ratios become progressively greater with increasing SiO_2 (Fig. 3). Sr isotopic compositions and $\delta^{18}O$ values also are generally higher in the Holocene dacites and rhyolites than in the more mafic lavas (Donnelly-Nolan, 1998). Sr isotopic compositions range from 0·70334 for the Giant Crater sample 82-72f (Baker *et al.*, 1991) and 0·70371 for the most primitive Callahan basalt (Kinzler *et al.*, 2000) to 0·70408 for the Pit Crater andesite (M. Lanphere and J. M. Donnelly-Nolan, unpublished data, 1985).

The variation in trace element concentrations and Sr–O isotopic compositions through the intermediate composition range at Medicine Lake has been explained by crystal fractionation of basaltic parent magmas combined with crustal assimilation, replenishment, and mixing [the FARM model of Baker *et al.* (1991)]. For example, silicic andesites of the Burnt Lava flow, which have compositions similar to those of the andesite enclaves in Glass Mountain rhyolites (see Table 1), were explained by fractionation of high-Al basalt combined with assimilation of crustal granitoids with an assimilation to crystallization rate exceeding unity (Grove *et al.*, 1997).

The andesitic samples from Katmai–Novarupta analyzed here have SiO_2 concentrations of 54·8–64·8 wt % and roughly parallel incompatible trace element patterns (Table 1; Fig. 4), suggesting that they had similar parental magmas, which differentiated along similar liquid lines of descent (Hildreth, 1987; Hildreth & Fierstein, 2000). Subducted materials were clearly involved in the genesis of each sample. Evidence for this includes enrichments in large ion lithophile and U-group elements (U, Th, and Pb) over LREE (e.g. Ba/La = 44–51; U/La = 0·10–0·13), and substantial depletions in Nb and Ta with respect to the LREE (e.g. La/Nb = 3·0–3·4; Table 1) in all samples.

Although the Cerberus and Falling Mountain dacites have trace element patterns similar to those of the 1912 dacite, they have somewhat lower concentrations of Zr and Hf, and they have lower U/Th ratios. The low Zr and Hf may reflect a separate differentiation path from the 1912 lavas. The lower U/Th ratios may reflect alteration of the older lavas.

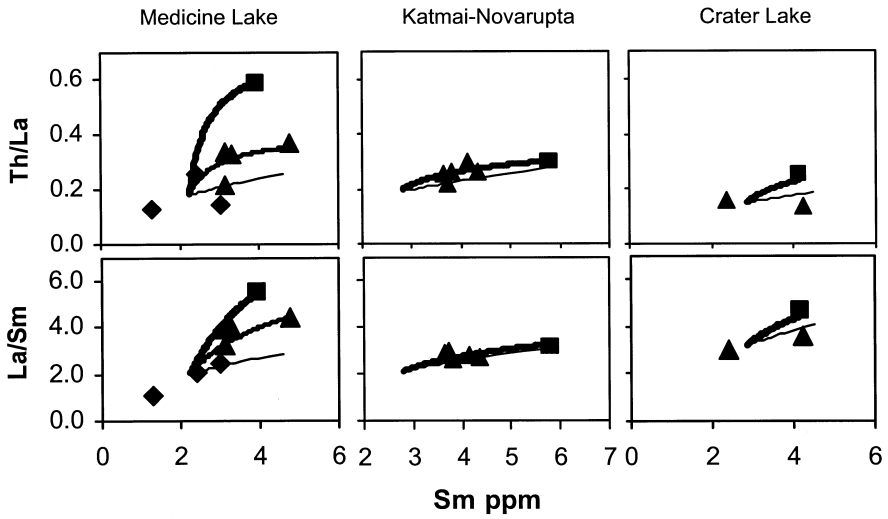

Fig. 3. Plot of Th/La and La/Sm vs Sm concentration (ppm) for samples from the Medicine Lake, Katmai–Novarupta, and Crater Lake volcanic systems. ◆, Basalts; ▲, andesites and dacites; ■, rhyodacites and rhyolites. Data are from Table 1. Fine lines represent Rayleigh crystal fractionation modeling. Bold lines represent EC-AFC modeling (see text for details). For the Medicine Lake system, the bold black line represents a model for the rhyolite; the line with an intermediate thickness represents a model for the andesites. Starting compositions used in the modeling are the average of the three basalts analyzed here for the Medicine Lake volcano, a hypothetical mafic parent magma for the Katmai–Novarupta region, and a mixture of $\frac{3}{4}$ low-Sr andesite 88c:1532 and $\frac{1}{4}$ high-Sr andesites 88c:1534 for Crater Lake. Partition coefficients used in the Rayleigh fractionation modeling: Th = 0, La = 0·25, and Sm = 0·5. Partition coefficients used for fractionating crystals in the EC-AFC models for the Katmai–Novarupta and Crater Lake systems: Th = 0·01, La = 0·15, and Sm = 0·25. Higher partition coefficients were used for generating the assimilants (Th = 0·3, La = 0·35, and Sm = 0·50), consistent with their relatively high silica contents, and the likelihood that they entrained crystals. Partition coefficients used for fractionating crystals in the EC-AFC models for the Medicine lake lavas: Th = 0·01, La = 0·07, and Sm = 0·2. Partition coefficients used for generating the assimilant: Th = 0·25, La = 0·25, and Sm = 0·40). Assimilant compositions used for Katmai–Novarupta: Th = 3·1 ppm, La = 11 ppm, and Sm = 4 ppm; for Crater Lake: Th = 4·9 ppm, La = 19 ppm, and Sm = 4·1 ppm; for Medicine Lake andesite: Th = 8 ppm, La = 20 ppm, and Sm = 5 ppm; for rhyolite: Th = 14 ppm, La = 20 ppm, and Sm = 3·35 ppm. The assimilant compositions are similar to those of recently erupted lavas from each volcanic center. The one exception is the assimilant composition used to model the Medicine Lake rhyolite, which is the composition of a granitic xenolith from the Glass Mountain rhyolite (85-25, M. K. Reagan, unpublished data, 2002). Other parameters employed in the EC-AFC modeling were the following: liquidus temperatures for magmas of 1200°C, liquidus temperatures for the assimilants of 1100°C, solidus temperatures for magmas and assimilants of 800°C, C_p for magmas of 1450 J/kg K, C_p for assimilants of 1370 J/kg K, enthalpy of crystallization of 390 kJ/kg, and enthalpy of fusion of 270 kJ/kg. The initial temperature of the assimilant was its solidus. The temperatures of the initial magmas were 1200°C for Medicine Lake and 1100°C for the other systems.

The similar SiO_2 concentrations and Fe/Mg ratios of the low- and high-Sr andesites (88c:1532 and 88c:1534, respectively) from Crater Lake indicate that they have undergone similar amounts of fractionation from their parental basalts (Table 1). However, the low-Sr andesite has lower concentrations of all highly incompatible elements (Fig. 5) but higher Ba/La (36 vs 23) and U/Th (0·49 vs 0·37) ratios, and lower Ce/Pb (3·8 vs 6·5) and K/Cs (8100 vs 10 500) ratios compared with the high-Sr andesite. All of these characteristics are consistent with a more significant contribution of a fluid from sediment-bearing subducting crust to the low-Sr andesite compared with the high-Sr andesite. The higher $^{87}Sr/^{86}Sr$ ratio of the low-Sr andesite compared with the high-Sr andesite (Bacon *et al*., 1994) also is consistent with this interpretation. The combination of high Sr isotopic compositions and low concentrations of incompatible elements in the low-Sr andesite is not consistent with greater crustal assimilation during differentiation of the low-Sr andesite compared with the high-Sr andesite. The low concentrations of HREE elements in both andesites imply that the mantle sources for the parental basalts for these andesites had a significant proportion of garnet (Bacon, 1990). Both of these andesites have elevated P and Sr contents compared with other incompatible elements (Fig. 5), providing clear evidence of accumulation of apatite and plagioclase, respectively (see Bacon & Druitt, 1988).

Rhyolites

The patterns of enrichment in the most highly incompatible elements such as the large ion lithophile elements (LILE) and Th for the rhyolitic rocks from all three centers are similar to those of associated more mafic rocks, showing that the rhyolites and rhyodacites are all genetically linked in some way to local young basalts and andesites. Differences in the degree to which isotopic compositions and ratios between more

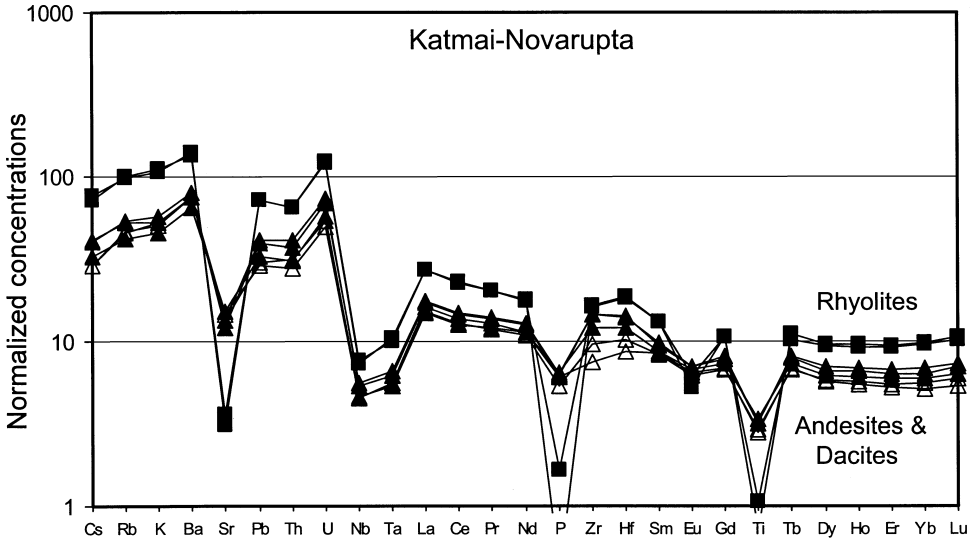

Fig. 4. Normalized incompatible trace element concentrations for volcanic samples from the Katmai–Novarupta region. Data are from Table 1. ■, 1912 rhyolite; ▲, 1912 silicic andesite and dacite from the 1912 eruption, as well as the 1961 Trident andesite; △, Cerberus and Falling Mountain dacites.

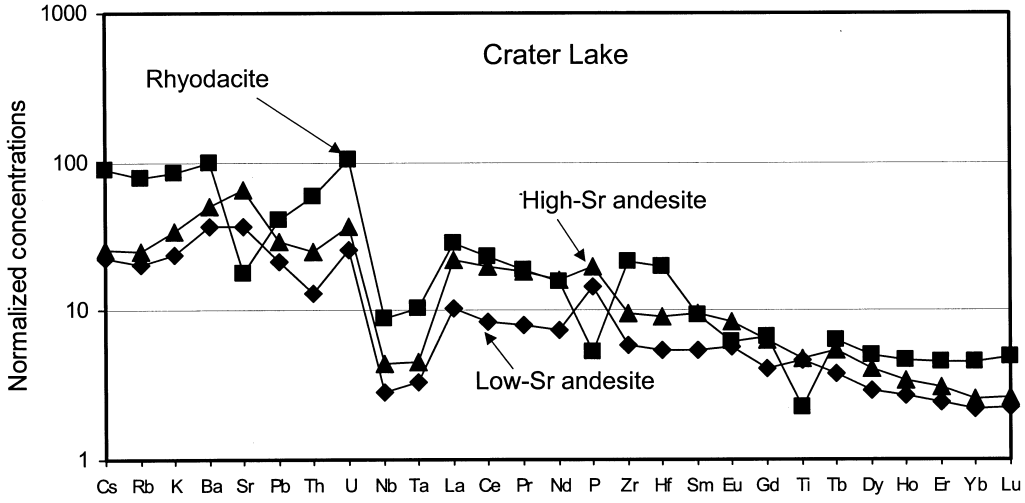

Fig. 5. Normalized incompatible trace element concentrations for samples from the Crater Lake climactic eruption. Data are from Table 1. ■, rhyolite; ▲, high-Sr andesite; ◆, low-Sr andesite.

and less incompatible elements shift with increasing silica show that the nature of the genetic link differs from center to center. For example, the Katmai–Novarupta rhyolites are characterized by incompatible trace element patterns that roughly parallel those of the andesites and dacites (Fig. 4), with little variation in Th/La and La/Sm ratios (Fig. 3), suggesting that the magmas are largely related by crystal fractionation (Hildreth, 1983, 1987). In contrast, trace element patterns of Medicine Lake rhyolites have significantly higher Th/La and La/Sm ratios compared with more mafic magmas (Fig. 3), and HREE concentrations that are identical to those of the basalts (Fig. 6). Average oxygen isotope values also are higher in the rhyolites than associated basalts (Donnelly-Nolan, 1998). These variations suggest that assimilation–fractional crystallization (AFC) processes link the basalts and rhyolites (Grove *et al.*, 1988, 1997). The processes linking Crater Lake rhyodacites to more mafic magmas may be a hybrid of those responsible for linking lava compositions for the Medicine Lake and Katmai–Novarupta centers. Evidence for this includes the

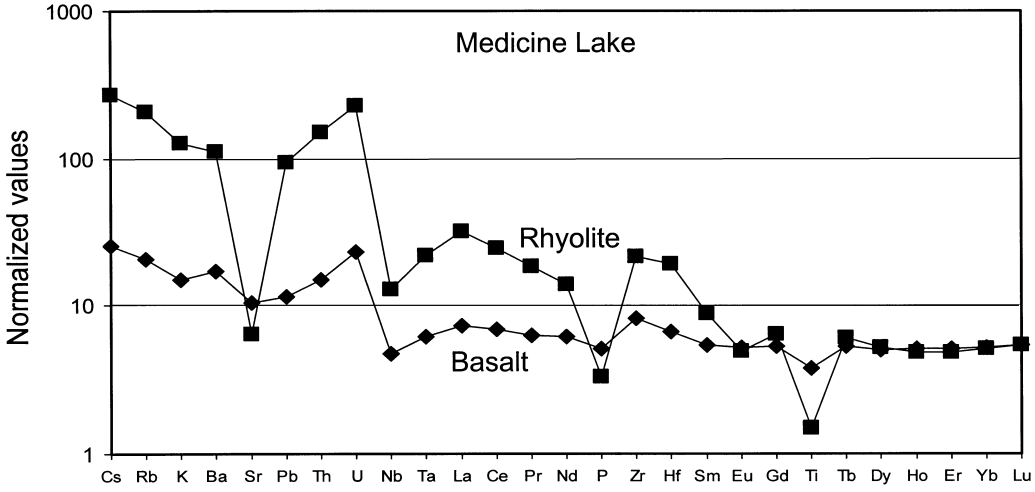

Fig. 6. Normalized incompatible trace element concentrations for the Black Crater basalt (733 m) and a Glass Mountain rhyolite (1368 m) from Medicine Lake volcano. Data are from Table 1.

strongly elevated Th/La ratio for the rhyodacite compared with the associated andesites (Fig. 3), despite the roughly similar incompatible trace element patterns for the andesites and rhyodacite (Fig. 5).

THORIUM AND URANIUM ISOTOPE ABUNDANCES

The Medicine Lake rhyolites plot on the equiline in Fig. 7, with $(^{230}Th)/(^{232}Th)$ ratios of ~1·21. Quenched and cumulate andesite enclaves from these young rhyolites, as well as recently erupted andesite to dacite lavas, have $(^{230}Th)/(^{232}Th)$ ratios of 1·08–1·18 and $(^{238}U)/(^{230}Th)$ values that depart from equilibrium by as much as 5% (Table 2). The degree of disequilibrium appears to be independent of whether the enclave has a cumulate or quenched texture. Basaltic samples have $(^{230}Th)/(^{232}Th)$ ratios more like those of the rhyolites than the andesites (1·17–1·21) and have near-equilibrium $(^{238}U)/(^{230}Th)$ values (Fig. 7). Ratios between U and Th nuclides in the Glass Mountain dacite lie between those for the rhyolite and a quenched andesite enclave (1545 m) extracted from the dacite, consistent with its origin by mixing (e.g. Eichelberger, 1981). Glass and magnetite separates from andesite enclave 1545 m were analyzed with a goal of obtaining its crystallization age (Table 2; Fig. 7). However, the fine grain size of this enclave limited the purity of the mineral separates and therefore the spread in $(^{238}U)/(^{232}Th)$ ratios.

Th isotopic compositions for all of the samples from Katmai–Novarupta are high (1·37–1·45, Table 2) despite varying $(^{238}U)/(^{232}Th)$ ratios, which probably is a reflection of the addition of U > Th and/or

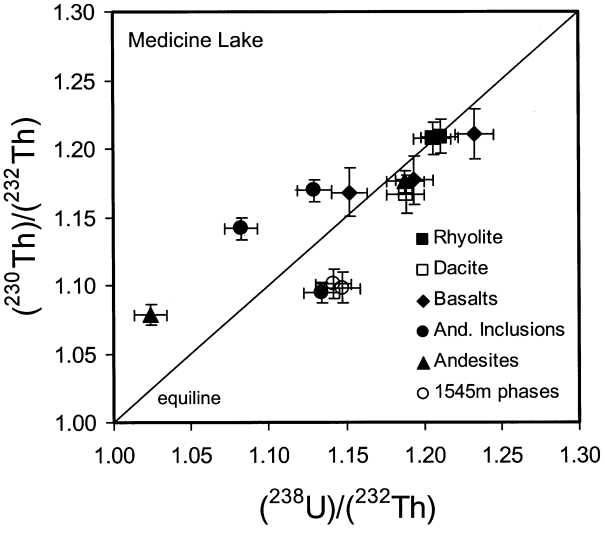

Fig. 7. Plot of $(^{230}Th)/(^{232}Th)$ vs $(^{238}U)/(^{232}Th)$ for samples from the Medicine Lake volcano. Data are from Table 2. The diagonal is the 'equiline' marking $(^{230}Th) = (^{238}U)$. □, Glass Mountain dacite. The phase separates from enclave sample 1545 m have compositions within error of the whole-rock values. It should be noted that the $(^{230}Th)/(^{232}Th)$ ratios for andesites are generally lower than those of basalts and rhyolites.

radiogenic Th from the subducting slab (see Thomas *et al.*, 2002). All intermediate whole-rock samples erupted in 1912 from the Katmai–Novarupta system have $(^{230}Th)/(^{232}Th)$ and $(^{238}U)/(^{232}Th)$ ratios that plot on or near a reference line yielding an age of ~40 ka (Table 2; Fig. 8). The $(^{238}U)/(^{232}Th)$ ratio appears to correlate positively with SiO_2 concentration for these samples. Separates of magnetite and pyroxene from the 1912 silicic andesite and dacite plot near the reference line for the intermediate whole rocks (Fig. 9).

Table 2: U–Th data for whole rocks and phase separates

	Type[1]	($^{238}U/^{232}Th$)	($^{230}Th/^{232}Th$)	($^{238}U/^{230}Th$)	($^{234}U/^{238}U$)	Th (ppm)	U (ppm)
Katmai–Novarupta[2]							
K90And	wr	1·378 ± 0·007	1·382 ± 0·011	0·997 ± 0·009	0·994 ± 0·007	3·361 ± 0·005	1·519 ± 0·013
K90And	wr	1·374 ± 0·006	1·385 ± 0·015	0·992 ± 0·011	1·006 ± 0·002	3·299 ± 0·010	1·484 ± 0·004
K90And	px	1·341 ± 0·006	1·392 ± 0·012	0·963 ± 0·006	1·002 ± 0·004	0·190 ± 0·001	0·0831 ± 0·0002
K90And	mag	1·440 ± 0·013	1·400 ± 0·011	1·028 ± 0·011	1·010 ± 0·006	0·959 ± 0·001	0·455 ± 0·004
K90Dac	wr	1·413 ± 0·009	1·407 ± 0·013	1·005 ± 0·002	0·997 ± 0·002	3·107 ± 0·018	1·437 ± 0·003
K90Dac	wr	1·429 ± 0·004	1·402 ± 0·018	1·015 ± 0·013	0·998 ± 0·004	3·008 ± 0·006	1·406 ± 0·003
K90Dac	mag	1·486 ± 0·007	1·417 ± 0·011	1·049 ± 0·007	0·997 ± 0·003	0·419 ± 0·002	0·205 ± 0·001
K90Dac	mag	1·506 ± 0·012	1·427 ± 0·025	1·055 ± 0·013	1·001 ± 0·005	0·419 ± 0·002	0·207 ± 0·001
K90Dac	px	1·422 ± 0·009	1·385 ± 0·020	1·027 ± 0·013	1·001 ± 0·005	0·433 ± 0·003	0·203 ± 0·001
K-851	wr	1·301 ± 0·006	1·361 ± 0·009	0·956 ± 0·007	1·000 ± 0·003	1·799 ± 0·005	0·771 ± 0·003
K90Rhy	wr	1·422 ± 0·007	1·440 ± 0·007	0·987 ± 0·006	1·000 ± 0·004	5·382 ± 0·012	2·521 ± 0·010
K90Nov	wr	1·430 ± 0·006	1·443 ± 0·011	0·991 ± 0·008	1·000 ± 0·005	5·368 ± 0·012	2·524 ± 0·009
K-2043	wr	1·384 ± 0·006	1·423 ± 0·011	0·973 ± 0·008	0·993 ± 0·007	3·305 ± 0·019	1·469 ± 0·006
K90TR	wr	1·412 ± 0·005	1·391 ± 0·015	1·016 ± 0·010	1·003 ± 0·003	2·628 ± 0·006	1·203 ± 0·002
K90CB	wr	1·317 ± 0·007	1·373 ± 0·011	0·959 ± 0·009	1·001 ± 0·005	2·485 ± 0·006	1·071 ± 0·005
K90FM	wr	1·366 ± 0·006	1·388 ± 0·019	0·984 ± 0·014	1·002 ± 0·004	2·250 ± 0·005	1·006 ± 0·004
K90FM	wr	1·364 ± 0·010	1·391 ± 0·017	0·981 ± 0·006	0·998 ± 0·002	2·413 ± 0·020	1·085 ± 0·003
Crater Lake[2]							
88c:1534	wr	1·167 ± 0·012	1·312 ± 0·011	0·890 ± 0·008	1·003 ± 0·002	2·077 ± 0·015	0·799 ± 0·006
88c:1534	mag[3]	1·199 ± 0·012	1·294 ± 0·008	0·926 ± 0·011	1·007 ± 0·006	0·847 ± 0·005	0·332 ± 0·002
88c:1534	gl	1·111 ± 0·009	1·306 ± 0·021	0·851 ± 0·013	0·998 ± 0·002	4·090 ± 0·030	1·488 ± 0·004
88c:1534	hblp	1·098 ± 0·007	1·284 ± 0·017	0·855 ± 0·011	0·995 ± 0·005	0·379 ± 0·003	0·136 ± 0·001
88c:1534	hblp	1·064 ± 0·015	1·292 ± 0·021	0·824 ± 0·006	0·998 ± 0·004	0·365 ± 0·005	0·128 ± 0·001
88c:1532	wr	1·557 ± 0·015	1·451 ± 0·017	1·073 ± 0·017	1·004 ± 0·015	1·012 ± 0·004	0·519 ± 0·005
88c:1532	pxh	1·482 ± 0·009	1·417 ± 0·013	1·046 ± 0·011	1·003 ± 0·012	0·274 ± 0·001	0·133 ± 0·001
88c:1532	pl	1·517 ± 0·011	1·430 ± 0·044	1·061 ± 0·033	0·997 ± 0·012	0·0313 ± 0·0002	0·0313 ± 0·0002
88c:1532	gl	1·576 ± 0·006	1·455 ± 0·009	1·083 ± 0·007	1·004 ± 0·002	2·463 ± 0·006	1·270 ± 0·004
88c:1533	wr	1·374 ± 0·010	1·368 ± 0·011	1·005 ± 0·009	1·006 ± 0·006	4·878 ± 0·013	2·193 ± 0·014
88c:1533	pl	1·485 ± 0·009	1·448 ± 0·017	1·025 ± 0·011	0·993 ± 0·005	0·1599 ± 0·0008	0·0777 ± 0·0003
Medicine Lake[3]							
82-72f	wr	1·153 ± 0·015	1·163 ± 0·022	0·991 ± 0·023	1·004 ± 0·003	0·179 ± 0·002	0·0676 ± 0·0003
1513 m	wr	1·194 ± 0·011	1·172 ± 0·024	1·018 ± 0·022		1·000 ± 0·009	0·391 ± 0·001
733 m	wr	1·233 ± 0·014	1·206 ± 0·019	1·023 ± 0·020	1·006 ± 0·008	1·235 ± 0·010	0·498 ± 0·006
1139 ma	wr	1·082 ± 0·013	1·137 ± 0·013	0·952 ± 0·016	1·001 ± 0·004	2·003 ± 0·008	0·710 ± 0·008
1545 m	wr	1·134 ± 0·012	1·090 ± 0·013	1·041 ± 0·017	0·998 ± 0·008	3·693 ± 0·024	1·371 ± 0·011
1545 m	wr				0·999 ± 0·004		1·358 ± 0·006
1545 m	mag	1·147 ± 0·004	1·094 ± 0·011	1·049 ± 0·011		4·526 ± 0·012	1·699 ± 0·004
1545 m	gl	1·142 ± 0·004	1·096 ± 0·018	1·042 ± 0·017	1·005 ± 0·001	5·336 ± 0·015	1·986 ± 0·006
1424ma	wr	1·130 ± 0·021	1·165 ± 0·005	0·970 ± 0·024	1·002 ± 0·003	3·974 ± 0·032	1·469 ± 0·026
695 m	wr	1·188 ± 0·005	1·171 ± 0·020	1·014 ± 0·018		5·252 ± 0·022	2·042 ± 0·004
945 m	wr	1·024 ± 0·012	1·074 ± 0·008	0·953 ± 0·013		7·314 ± 0·036	2·450 ± 0·026
945 m	wr	1·024 ± 0·004				7·321 ± 0·014	2·453 ± 0·008
1413 m	wr	1·188 ± 0·010	1·162 ± 0·013	1·023 ± 0·014	1·001 ± 0·005	7·453 ± 0·022	2·898 ± 0·025
1368 m	wr	1·210 ± 0·002	1·204 ± 0·010	1·005 ± 0·009	1·002 ± 0·003	12·539 ± 0·096	4·967 ± 0·010
1331 m	wr	1·206 ± 0·001	1·203 ± 0·014	1·002 ± 0·012	1·000 ± 0·001	13·650 ± 0·086	5·385 ± 0·004

Table 2: continued

	Type[1]	(^{238}U/^{232}Th)	(^{230}Th/^{232}Th)	(^{238}U/^{230}Th)	(^{234}U/^{238}U)	Th (ppm)	U (ppm)
TML[4]	wr[2]	1·063 ± 0·006	1·079 ± 0·013	1·010 ± 0·012	0·997 ± 0·004	29·500 ± 0·100	10·270 ± 0·050
TML[4]	wr[3]	1·073 ± 0·007	1·075 ± 0·009	0·998 ± 0·011	1·003 ± 0·003	30·060 ± 0·090	10·560 ± 0·060

Decay constants used (see Cheng *et al.*, 2000): ^{234}U, $2{\cdot}826 \times 10^{-6}$; ^{238}U, $1{\cdot}55125 \times 10^{-10}$; ^{230}Th, $9{\cdot}158 \times 10^{-06}$; ^{232}Th, $4{\cdot}948 \times 10^{-11}$.
[1]wr, whole-rock powder; gl, glass; pl, plagioclase; mag, magnetite; px, pyroxene; pxh, pyroxene with minor hornblende; hblp, hornblende with minor pyroxene.
[2]Analyzed at the Minnesota Isotope Laboratory.
[3]Analyzed at Woods Hole Oceanographic Institution.
[4]Table Mountain Latite standard.

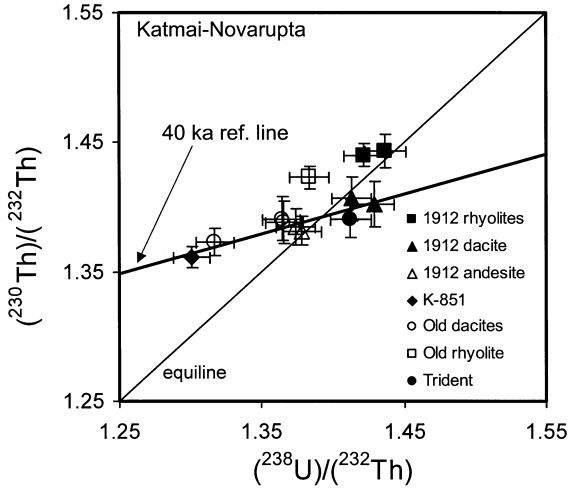

Fig. 8. Plot of (^{230}Th)/(^{232}Th) vs (^{238}U)/(^{232}Th) for whole-rock samples from the Katmai–Novarupta volcanic system. Data are from Table 3. The Cerberus and Falling Mountain dacites are both highly oxidized, and their enrichment in ^{230}Th may reflect U loss during oxidation. It should be noted that all intermediate whole rocks and phase separates plot near a single reference line with an age of ~40 ka. All rhyolitic samples fall off of this trend.

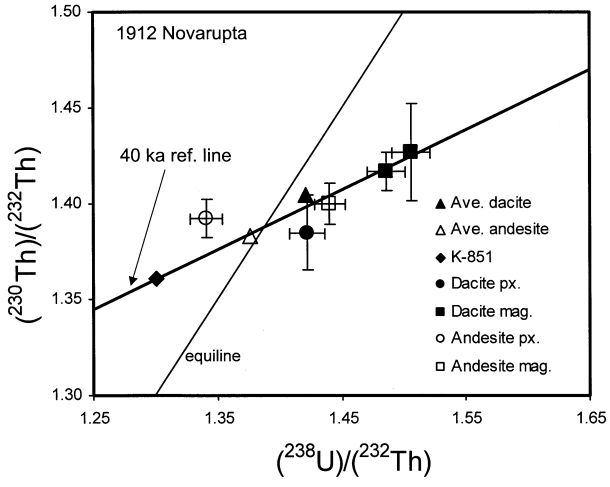

Fig. 9. Plot of (^{230}Th)/(^{232}Th) vs (^{238}U)/(^{232}Th) ratios for whole rocks and phase separates from the silicic andesite and dacite erupted in 1912 from Novarupta. Data are from Table 2. The continuous diagonal line represents the same 40 ka reference line as shown in Fig. 8.

These separates have U and Th concentrations that are significantly less than whole-rock values. Pyroxene separates have (^{238}U)/(^{232}Th) ratios that are similar to those of the whole rocks, whereas magnetite separates have significantly higher (^{238}U)/(^{232}Th) ratios (Table 2).

The 1912 rhyolites have higher (^{230}Th)/(^{232}Th) ratios than the intermediate samples. The tephra sample (K90Rhy) has a 1% excess of (^{230}Th) over (^{238}U), which may reflect recent zircon fractionation (see Hildreth & Fierstein, 2000). The 72 wt % SiO_2 rhyolite from the crater walls of Mount Katmai (K-2043), which has been dated at 22 ka (Hildreth & Fierstein, 2000), has a Th isotopic composition between those of the 1912 rhyolite and the intermediate Katmai–Novarupta rocks. Age-corrected (^{230}Th)/(^{232}Th) values for the Cerberus and Falling Mountain dacites would plot in the same range as this rhyolite, perhaps linking these dacites petrogenetically with this rhyolite. However, the low (^{238}U)/(^{230}Th) ratios for these samples may have resulted from alteration. If so, then the age correction for the (^{230}Th)/(^{232}Th) values would not be valid.

The degree of disequilibrium between ^{238}U and ^{230}Th in the climactic andesites from Crater Lake is greater than for any of the other mafic to intermediate samples reported here (Table 2, Fig. 10). The low-Sr andesite has a relatively high (^{230}Th)/(^{232}Th) ratio (1·45) and (^{238}U)/(^{230}Th) = 1·07, whereas the high-Sr andesite has a lower (^{230}Th)/(^{232}Th) ratio (1·32) and (^{238}U)/(^{230}Th) = 0·89.

The mineral separates from the high-Sr andesite have a narrow range in Th isotopic composition, and a spread in (^{238}U)/(^{232}Th) ratios of ~8% (Fig. 10). The (^{230}Th)/(^{232}Th) and (^{238}U)/(^{232}Th) ratios for the whole rock and phase separates from this sample plot

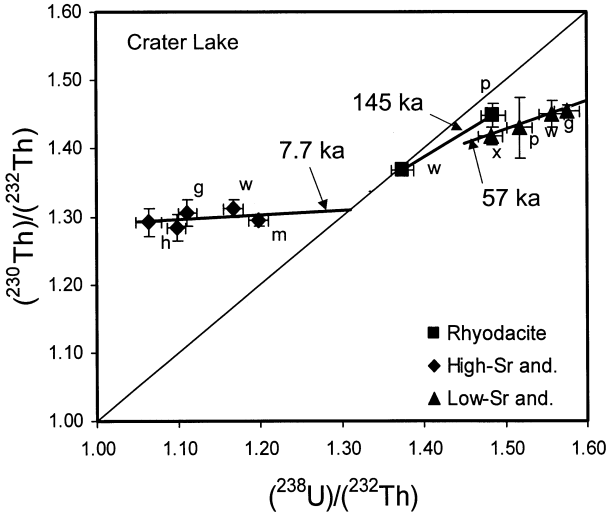

Fig. 10. Plot of $(^{230}Th)/(^{232}Th)$ vs $(^{238}U)/(^{232}Th)$ for samples from the Crater Lake volcanic system. Data are from Table 2. w, whole-rock values; p, plagioclase; x, pyroxene (with minor hornblende); h, hornblende (with minor pyroxene); m, magnetite; g, glass. It should be noted that the whole rock and phase separates for the high-Sr andesite plot within error of a reference line with an age equal to that since the climactic eruption. The internal 'isochrons' for the high-Sr andesite and rhyolite give similar ages of 57(+18/−17) and 145(+55/−38) ka, respectively, using the Yorkfit routine of the Isoplot program (Ludwig, available at http://www.bgc.org/Isoplot2·49Manual.pdf).

near a 7·7 ka reference line representing the time since eruption. In contrast, the best-fit reference line drawn through the mineral separates for the low-Sr andesite gives an age of 57 ka. If these crystals grew from low-Sr magmas, then the difference in Th isotopic composition between the low- and high-Sr andesites may be attributed to a long crustal residence time for the melts and crystals making up the low-Sr andesite.

The climactic rhyodacite from Crater Lake has $(^{230}Th)/(^{232}Th) = 1·37$ and an equilibrium $(^{238}U)/(^{230}Th)$ ratio. In contrast to Medicine Lake and Katmai–Novarupta, however, the rhyodacite from Crater Lake has $(^{230}Th)/(^{232}Th)$ and $(^{238}U)/(^{232}Th)$ ratios between those of the associated andesites (Fig. 10). A plagioclase mineral separate from this rhyolite has a $(^{230}Th)/(^{232}Th)$ ratio similar to that of the low-Sr andesite.

LEAD ISOTOPE ABUNDANCES

Intermediate and silicic rocks from the three volcanic systems studied here collectively have a narrow range of Pb isotope compositions (Table 3), similar to those for lavas from other arcs. The data fall near the Northern Hemisphere reference line (NHRL) on plots of $^{208}Pb/^{204}Pb$ vs $^{206}Pb/^{204}Pb$, but form a steep trend towards local subducting sediments on plots of $^{207}Pb/^{204}Pb$ vs $^{206}Pb/^{204}Pb$ (Fig. 11). The samples from the

Table 3: Pb isotope data for whole rocks

	$^{206}Pb/^{204}Pb$	$^{207}Pb/^{204}Pb$	$^{208}Pb/^{204}Pb$
Medicine Lake			
1545m	19·0146	15·6136	38·6870
1139ma	19·0001	15·6117	38·6730
1543m	19·0084	15·6124	38·6885
1331m	18·9019	15·6060	38·6293
733m	18·9046	15·6044	38·6475
Katmai–Novarupta			
K90Rhy	18·8511	15·5732	38·3751
K90Dac	18·8802	15·5691	38·3806
Crater Lake			
88c:1533	18·9291	15·5981	38·5702
88c:1532	18·8876	15·5850	38·5128
88c:1534	18·8361	15·5935	38·4963
Average 1σ error (%)	0·0013	0·0013	0·0021

Katmai–Novarupta system have Pb isotope values that plot closest to those of oceanic mantle values, whereas the Medicine Lake samples plot closer to those of North Pacific sediment. Thus, although the slab contribution to the magma sources for Medicine Lake lavas appears to be less than for the other centers based on trace element concentrations, the proportion of sediment in this component appears to be higher for Medicine Lake lavas.

Samples from individual centers have narrow ranges in Pb isotope compositions that vary independently of SiO_2 content (Table 3). For example, Medicine Lake rhyolite and basalt have identical Pb isotope values, whereas andesites have slightly more radiogenic values. The implied long-term time-integrated U/Th ratios for the sources of the basalt and rhyolite are lower than for the sources for the andesites, which is the opposite of the time-integrated U/Th ratios inferred from the $(^{230}Th)/(^{232}Th)$ ratios (see Fig. 7). The Crater Lake rhyolite has slightly more radiogenic Pb isotopic compositions compared with the andesites (Table 3). Nevertheless, these within-suite differences in Pb isotopic composition are minor, and taken as a group, the Pb isotopes place little constraint on the amount of assimilation of continental crust needed to produce silicic magmas in these systems.

DISCUSSION

Assimilation of plutonic materials during differentiation of calcalkaline magmas can be difficult to detect if

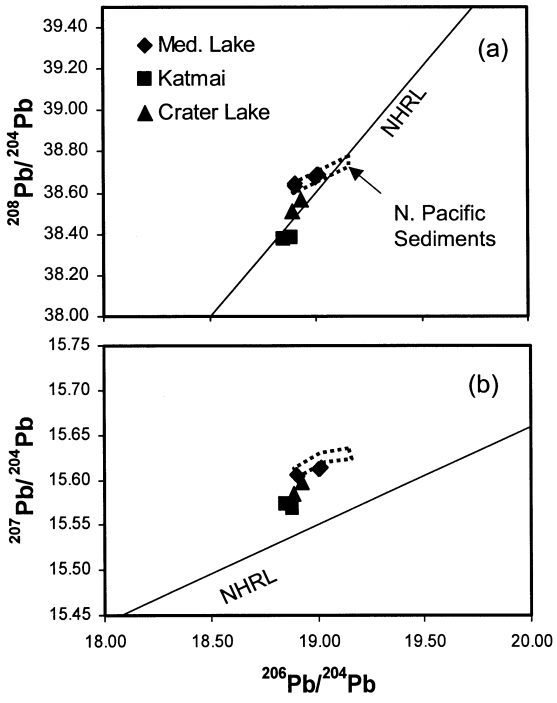

Fig. 11. Plot of $^{208}Pb/^{204}Pb$ (a) and $^{207}Pb/^{204}Pb$ (b) vs $^{206}Pb/^{204}Pb$ for samples from the Medicine Lake, Crater Lake, and Katmai–Novarupta volcanic systems. The field for averaged sediments from the northern Pacific sea floor is shown (Plank & Langmuir, 1998). NHRL, Northern Hemisphere reference line (Hart, 1984).

the material assimilated has a major element, trace element, and isotopic composition that is similar to that of the magmas. Heat and volatile transfer from magmas intruding into recently crystallized magmatic rocks or crystal mushes of similar composition could cause significant melting (Bergantz, 1995). Mixing between the remelted 'assimilant' and a newly intruded magma batch would result in a magma containing both old and young crystals with differing morphologies (e.g. Coombs *et al.*, 2000), but incompatible trace element and isotopic compositions largely unaffected by the mixing event. Detection of such 'cryptic assimilation' is difficult for most isotopic tracers because little or no material with a distinct isotopic composition is added to the system. Th isotopes, however, are an exception because of the relatively rapid response of the $(^{230}Th)/(^{232}Th)$ ratio to varying U/Th ratios. Differences in Th isotopic composition between mineral separates in a volcanic rock can be used to provide important clues about the time-scales of magma generation or differentiation at a volcanic center.

In the following discussion, trace element and isotope variations are used to show that cryptic assimilation of previously crystallized material is an important process in the differentiation of the magmas studied here. These variations are also used to test the hypothesis that progressively longer time-periods of mafic magmatism are required to generate progressively more silicic magmas in these large magmatic systems.

Katmai–Novarupta

The mafic andesite erupted from the Novarupta vent in 1912 (K-851) is enriched in (^{230}Th) over (^{238}U) by 4% (Fig. 8), despite high Th isotopic compositions and other evidence for the presence of a subducted component in these lavas. Thus, the subducted slab components were probably added to the mantle source of the parental basalts long before melting, and recent melting of this source with garnet or aluminous clinopyroxene in the residue probably produced parental basalts in this system (e.g. LaTourette *et al.*, 1993; Blundy, 1998; Landwehr *et al.*, 2001). The relatively high HREE concentrations for Katmai–Novarupta lavas are most consistent with residual aluminous clinopyroxene in the source rather than garnet. An alternative explanation is that the (^{230}Th) excess resulted from assimilation. However, as shown below, assimilation leading to generation of silicic andesites and dacites appears to drive the compositions towards higher $(^{238}U)/(^{230}Th)$ ratios in the Katmai–Novarupta system.

The trends to higher $(^{238}U)/(^{232}Th)$ and $(^{230}Th)/(^{232}Th)$ ratios with increasing SiO_2 for the 1912 silicic andesites and dacites erupted in 1912 from the Katmai–Novarupta system (Fig. 8) appear to have resulted from cryptic assimilation combined with fractional crystallization. The pyroxene and magnetite mineral separates from the dacite and silicic andesite erupted in 1912 have U and Th concentrations that are significantly lower than whole-rock values and $(^{238}U)/(^{232}Th)$ ratios that are too high to explain variations in the U/Th ratios of the whole rocks. Apatite fractionation, which clearly occurred in this system (see Fig. 4), may affect $(^{238}U)/(^{232}Th)$ ratios and explain this correlation. However, it should be noted that U and Th concentrations and Th/U ratios for apatites from Crater Lake andesites are not high enough to affect this change (see below). Nevertheless, it is possible that these trends resulted from the addition of an assimilant during crystal fractionation that was extracted from residual crust with apatite or another trace mineral with relatively high U/Th. In any case, the lack of significant variations in the patterns of other trace elements and Sr–O isotopic compositions for the andesites and dacites (Hildreth, 1987) suggests that the assimilant involved in generating the intermediate Katmai–Novarupta magmas had a composition generally similar to the magmas themselves.

Trace element abundances in these intermediate rocks were modeled using an energy constrained AFC model (EC-AFC; Bohrson & Spera, 2001; Spera & Bohrson, 2001). Parameters used in the modeling assume that the assimilant was similar in composition to recent volcanics, and that it was at its solidus at the beginning of fractionation (Fig. 3). The partition coefficients for incompatible elements between residual crystals and melts of the assimilant were chosen to be significantly higher than the partition coefficients for crystallizing the magmas. This choice mimics assimilation of a significant portion of the residual crystals along with the magma, which is consistent with the abundance of crystals with complex growth and resorption textures in intermediate Katmai–Novarupta lavas. The positions of bulk mineral separates from the 1912 silicic andesite and dacite along the U–Th 40 ka isochron with whole rocks (Fig. 9) also are consistent with this model, and indicate that the average ages of the crystals in these magmas must be similar to the average crustal residence time of the aggregated magmas themselves.

The 1912 rhyolites from the Katmai–Novarupta system have high concentrations of incompatible trace elements, with patterns that are similar to those of the andesites and dacites (Fig. 4). This pattern of enrichment is consistent with generation of the rhyolite by crystal fractionation of intermediate magmas like those erupted in 1912 with only minor assimilation (Hildreth, 1987; Hildreth & Fierstein, 2000). In addition, the similar Pb and oxygen isotope compositions for the rhyolites and dacites are consistent with, at most, ~1% assimilation of sedimentary or pre-Cenozoic granitoid rocks (e.g. Hildreth, 1997). It is also possible that the rhyolites were generated by a continuation of the cryptic AFC process that explained the composition of the 1912 dacite. That is, crystal fractionation and assimilation of rocks or crystal mushes with compositions like the magmas themselves also can explain the compositions of the rhyolites (Fig. 3).

Both explanations require a period of enrichment in U over Th of 10^5 years or more to generate the distinctively high $(^{230}Th)/(^{232}Th)$ ratios of the rhyolites (Fig. 8). In addition, the small excess in ^{230}Th over ^{238}U in the rhyolites despite their high $(^{230}Th)/(^{232}Th)$ ratios indicates that fractionation of a trace amount of zircon probably occurred shortly before eruption (see also Hildreth & Fierstein, 2000).

The $(^{230}Th)/(^{232}Th)$ and $(^{238}U)/(^{232}Th)$ ratios for the rhyolite (K2043) from the Katmai crater walls plot between values for these ratios in the 1912 rhyolite and andesite samples (Fig. 8). The two rhyolites, therefore, may be genetically linked, with the principal difference between them being the presence of 'inmixed' andesite magma in the Katmai rhyolite. This link provides further evidence that the 1912 rhyolite resided beneath Katmai before the 1912 eruption, and its withdrawal during the eruption led to the collapse of the Katmai summit (see Hildreth & Fierstein, 2000).

Medicine Lake

All of the Medicine Lake basalts have near-equilibrium $(^{238}U)/(^{230}Th)$ ratios (Table 2, Fig. 7), including the relatively primitive high-alumina basalt from Giant Crater and the more differentiated Black Crater and Callahan calcalkaline basalts. These data are consistent with experimentally determined shallow equilibration pressures for primitive Medicine Lake basalts within the mantle (Tanton *et al.*, 2001), with the partition coefficients for U and Th between melts and residual mantle being roughly equal (e.g. Beattie, 1993; LaTourrette *et al.*, 1993; Wood *et al.*, 1999; Landwehr *et al.*, 2001).

Geological, trace element, and isotopic data, including the progressively steeper REE patterns and higher $^{87}Sr/^{86}Sr$ and $\delta^{18}O$ with increasing SiO_2 in Medicine Lake lavas, have been attributed to AFC processes (Grove *et al.*, 1988; Donnelly-Nolan, 1998). The lower $(^{230}Th)/(^{232}Th)$, higher $^{206}Pb/^{204}Pb$, and more diverse $(^{238}U)/(^{230}Th)$ ratios for Medicine Lake andesites compared with basalts are consistent with this view. The assimilants probably included more significant proportions of older crustal materials than for the other systems studied here as evidenced by the variation in Sr and O isotope data between basalts and andesites (Donnelly-Nolan, 1998). The low $(^{230}Th)/(^{232}Th)$ ratios in lavas indicate that the average U/Th ratio of the assimilant is lower than present-day basaltic values. The variation in the $(^{238}U)/(^{230}Th)$ ratios for the andesites suggests that these assimilants were generated by melting crust, leaving a residue with variably fractionated U from Th (Fig. 7). U/Th ratios are highly variable in granitic xenoliths from Medicine Lake lavas (Lowenstern *et al.*, 2000), including those with low enough values to be assimilants involved in generation of the andesites.

Low HREE concentrations for the andesites (Fig. 2) require relatively high partition coefficients for these elements during differentiation. The fractionated HREE patterns require either that these partition coefficients progressively increase with atomic number to values greater than unity for Yb or that the assimilant had fractionated HREE patterns. Based on experimental evidence (e.g. Gill, 1981), it is unlikely that an assemblage including a phase with strongly varying partition coefficients for HREE (e.g. zircon and garnet) could fractionate from the basalts or andesites at Medicine Lake at crustal pressures. Thus, EC-AFC

modeling of the andesitic compositions utilized an assimilant with a strongly fractionated HREE pattern (Fig. 3). The disequilibrium $(^{238}U)/(^{230}Th)$ ratios, but scattered $(^{230}Th)/(^{232}Th)$ ratios, for the andesites only constrain the time-scales required for their generation and differentiation to be less than a few hundred thousand years.

The Glass Mountain rhyolite has the peculiar trait of having Pb and Th isotope values identical to those of the young Medicine Lake basalts, but different from those of the young andesites, including the andesitic inclusions extracted from the rhyolite itself (Figs 7 and 11). The implication is that the rhyolite is more akin to the basalts than to the andesites. However, as with the andesites, variations in $\delta^{18}O$ values between Holocene basalts (average 5·7) and rhyolites (average 7·4) suggest that at least a small portion of crustal materials, other than young mafic plutons, must have been involved in the genesis of these rhyolites (Donnelly-Nolan, 1998). Nevertheless, the overall similarity of the patterns in highly incompatible trace elements as well as Th and Pb isotopic compositions between the rhyolite and basalt (Figs 6, 7 and 11) suggest that the principal sources of mass in the rhyolite were the Medicine Lake basalts. Therefore, the most likely origin for the Medicine Lake rhyolite is crystal fractionation of basalt combined with assimilation of some crustal material with an elevated $\delta^{18}O$ value (see Fig. 3). Based on the similar degree of enrichment of Zr and Ce in the rhyolite compared with the basalts (Fig. 6) and the similar HREE contents in the Medicine Lake basalts and rhyolites, hornblende probably played a major role in producing the Medicine Lake rhyolites.

The apparent differences in the nature of the crustal materials involved in magma genesis suggest that the andesites and rhyolites were generated in different places in the crust. The andesites were probably generated at depths of 6 km or more (see Grove *et al.*, 1997), whereas the rhyolites last equilibrated at depths of 1–3 km (Zucca *et al.*, 1986; Brophy *et al.*, 1996; Grove *et al.*, 1997).

Crater Lake

The high-Sr andesite is enriched in ^{230}Th over ^{238}U and has a relatively low $(^{230}Th)/(^{232}Th)$ ratio, whereas the low-Sr andesite has $(^{238}U) > (^{230}Th)$ and a significantly higher $(^{230}Th)/(^{232}Th)$ ratio (Fig. 10). The high-Sr andesite is also distinguished from the low-Sr andesites by significantly lower Sr isotopic compositions and incompatible trace element ratios suggesting less involvement of fluids from subducted slabs in magma genesis. These observations allow the differences in the compositions of the andesites to be largely the result of variations in the proportions of fluid from subducting lithosphere involved in the genesis of their parental magmas. The high concentrations of highly incompatible trace elements in the high-Sr andesite, its steep REE pattern, and low $(^{238}U)/(^{230}Th)$ value probably reflect low degrees of partial melting of a garnet-bearing (Beattie, 1993; LaTourrette *et al.*, 1993) or aluminous augite-bearing (Blundy, 1998) mantle source to generate its parental basalt. In contrast, the low concentrations of incompatible trace elements and stronger subduction signal in the low-Sr andesite, including its high $(^{238}U)/(^{230}Th)$ ratio, suggest that its parent basalt was generated by a greater degree of melting because of a significant flux of subducted fluid (see Bacon *et al.*, 1994; Stolper & Newman, 1994; Hirschmann *et al.*, 1999; Eiler *et al.*, 2000).

High normalized concentrations of Sr and P relative to other incompatible elements suggest that both andesites may have accumulated crystals (Fig. 5; Bacon & Druitt, 1988). Nevertheless, the abundances of U, Th, and other highly incompatible elements in these andesites cannot be attributed to crystal accumulation because the major phenocryst phases in these samples have low concentrations of these elements (Table 2). This is also true for the trace phase apatite, as only ~0·5 wt % apatite accumulation is needed to produce the excess phosphorus in the high-Sr and low-Sr andesites, and these apatites have low U and Th concentrations (1·8 and 4·6 ppm, respectively; R. Thomas & M. Reagan, unpublished data, 2001). Thus, the differences in the U–Th systematics and incompatible trace element abundances between the low- and high-Sr andesites must largely reflect differences in the compositions of their glass phases (see also Bacon & Druitt, 1988).

Based on geological mapping and geochronology, Bacon & Druitt (1988) suggested that low-Sr magmas crystallized at depth and fed rhyodacitic magmas into the developing climactic magma chamber for several tens of thousands of years before the climactic eruption of Mount Mazama. High-Sr magmas were suggested to have entered the chamber system shortly before the climactic eruption. The U–Th data for the andesites are consistent with this model. For example, the high U/Th ratio and Th isotopic composition of low-Sr andesite sample 88c:1532 is consistent with a significant residence time in the crust. In addition, the inclined U–Th reference line in Fig. 10 for mineral separates from 88c:1532 indicates that most crystals in this andesite grew from low-Sr andesite magma tens of thousands of years before eruption. The minimum age of this growth is 57(+18/–17) ka based on the slope of the reference line and the assumption that all of the crystals grew instantaneously upon intrusion into the crust. If crystals in 88c:1532 grew over time as the magma cooled, or were recycled from older magma

batches, then sample 88c:1532 could have resulted from magmatism that extended past this age. The complex morphologies of most of the plagioclase crystals in the sample of the low-Sr andesite are consistent with an extended and complex history of crystallization and resorption.

The best-fit line through the U–Th data for the high-Sr andesite (88c:1534) gives an age that is within error of the eruption age (Fig. 10), suggesting that this andesite intruded into the system within a few thousand years of the climactic eruption. The quench-textured morphologies of the hornblendes and the simpler zoning profiles for a majority of the plagioclase in 88c:1534 are consistent with this relatively short average residence time for most crystals in this andesite.

At this point, it should be noted that both of the andesitic samples are exceedingly crystalline, and they must have been fairly rigid before they erupted as scoria blocks. Thus, the applicability of the residence times inferred from the U–Th isochron plot to other scoria blocks, even those with similar compositions, would depend on how systematically stratified these crystal mushes were before eruption. If the andesites intruded in sequence at the andesite–rhyodacite boundary as suggested by Bacon & Druitt (1988), then the erupted low-Sr andesites would have been younger than the low-Sr andesites left behind in the chamber. Conversely, if andesitic magmas randomly intruded themselves within pre-existing crystal mushes, then the residence times inferred for the andesite samples would be more representative of the Crater Lake andesites as a whole. The complex morphologies of the crystals in the low-Sr andesite suggest that the latter is more probable than the former.

The major element, trace element, isotope, and U-series data (Tables 1 and 2; Fig. 10) for the climactic rhyodacite are consistent with its genesis by mixing of crystal fractionation products of associated low- and high-Sr andesites with minor assimilation of granitic wall-rocks (Bacon & Druitt, 1988). Note, however, that an EC-AFC model employing an assimilant composition like that of the Crater Lake rhyolite also explains the data (Fig. 3). Both models allow the equilibrium $(^{238}U)/(^{230}Th)$ ratio for the rhyolite to have resulted from fortuitous mixing proportions of low- and high-Sr components. An alternative and perhaps less fortuitous explanation for the U–Th equilibrium is that the rhyodacite resided in the crust for a period of $>10^5$ year. The extended age (140 ka) of the internal reference line for the climactic rhyodacite is consistent with this second explanation. However, most plagioclase crystals in the climactic rhyodacite have low-Sr affinities (Druitt & Bacon, 1989), and the plagioclase may have grown in a low-Sr rhyodacitic magma before high-Sr magmas began intruding into the system.

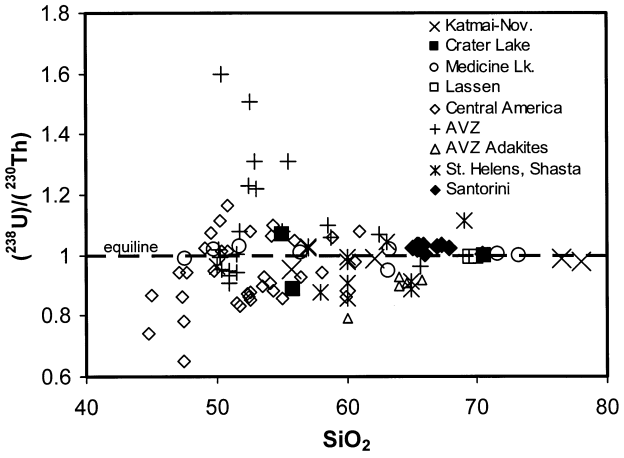

Fig. 12. Variation of $(^{238}U/^{230}Th)$ vs SiO_2 for volcanic rocks from continental arcs built on thickened crust. Data sources: this work; Lassen, M. K. Reagan (unpublished data, 2002); Shasta, Volpe (1992); St. Helens, Volpe & Hammond (1991); Central America, Reagan *et al.* (1994), Herrstrom *et al.* (1995) and M. K. Reagan (unpublished data, 2002); Santorini (Zellmer *et al.*, 2000); the Austral Volcanic Zone (AVZ), Hickey-Vargas *et al.* (2002) and Sigmarsson *et al.* (2002). Adakites from the Austral Volcanic Zone in Chile (Sigmarsson *et al.*, 1998) are plotted separately. The wide-ranging ^{238}U–^{230}Th disequilibrium in basalts and basaltic andesites and the progressive decrease in these ratios with increasing SiO_2 should be noted. The dacitic rocks from Mount St. Helens that are thought to be melts of basaltic crust (Halliday *et al.*, 1983; Smith & Leeman, 1987) appear to be exceptions to this overall trend. The general implication of these data is that generation of rhyolites in continental crust commonly involves persistent basaltic magmatism to generate silicic andesite to dacite compositions and crustal residence times for rhyolites that are significantly greater than the half-life of ^{230}Th (see text).

Based on these arguments, it is not possible to uniquely constrain the crustal residence time of the Crater Lake rhyodacite.

Geochemical relationships

Basalts from many volcanic arcs erupt with significant U–Th disequilibrium produced during mantle melting (Fig. 12). Some are enriched in ^{238}U over ^{230}Th by as much as a factor of two, reflecting the addition of U > Th to mantle sources from subducting slabs (e.g. Sigmarsson *et al.*, 1990; Gill *et al.*, 1993; Reagan *et al.*, 1994; Elliott *et al.*, 1997; Turner *et al.*, 2000*b*). Less common are arc basalts that are enriched in ^{230}Th over ^{238}U. These basalts have been attributed to small degrees of melting in the presence of garnet or aluminous augite and a small flux from subducting lithosphere (e.g. Reagan & Gill, 1989; Clark *et al.*, 1998; Turner *et al.*, 2000*a*). Basalts with equilibrium $(^{238}U)/(^{230}Th)$ ratios also are relatively common in volcanic arcs (Condomines & Sigmarsson, 1993).

The $(^{238}U)/(^{230}Th)$ disequilibria and trace element contents of the basalts and basaltic andesites from the volcanic centers investigated here appear, at least partially, to preserve a record of the processes that generated their parental magmas by melting mantle. The equilibrium values of Medicine Lake basalts provide no information about the time-scales of transport to the surface. However, the disequilibrium $(^{238}U)/(^{230}Th)$ ratios of the Katmai–Novarupta basaltic andesite and the high-Sr basaltic andesite from Crater Lake indicate that magma storage, differentiation, and transport to the surface require significantly less than a few hundred thousand years. In most arc settings, young basalts have significant enrichments in ^{226}Ra over ^{230}Th, suggesting that they rise from their mantle source, differentiate, and erupt in time periods of no more than $\sim 10^3$ years (Reagan *et al.*, 1994; Clark *et al.*, 1998; Turner *et al.*, 2000*b*, 2001; Hickey-Vargas *et al.*, 2002; Sigmarsson *et al.*, 2002).

The variations in $(^{230}Th)/(^{232}Th)$ and $(^{238}U)/(^{232}Th)$ in intermediate magmas at all three centers require significant assimilation in their genesis. The low-Sr andesite from Crater Lake and the andesites and dacites from the Katmai–Novarupta center were apparently generated by crystal fractionation and assimilation of mixtures of crystals and melts with incompatible trace element and isotopic compositions recently derived from the mantle. The average residence times for the crystals in these systems are in the range of tens of thousands of years. Differentiation of basaltic magmas to generate andesites recently erupted from Medicine Lake volcano also requires significant assimilation. However, changes in isotopic composition in progressively more differentiated magmas require that the assimilant included a somewhat more significant proportion of older crust.

The low amounts of $(^{238}U)/(^{230}Th)$ disequilibrium found in silicic andesites in contrast to the higher levels of disequilibrium in basaltic parents suggest a long time-period of fractionation, assimilation of equilibrated crust, or both (Fig. 12). The data shown here suggest that the silicic andesites and dacites are generated by tens of thousands of years or more of intrusion of basalt in the crust. Differentiates of old basalts are partially digested and assimilated by younger magmas. The effect on whole-rock compositions is to generally lower the degree of $(^{238}U)/(^{230}Th)$ disequilibrium, although in some cases, fractionation of crystals from liquids in the assimilant can enhance this disequilibrium. In any case, the resulting mixtures of melts and crystals produce averaged U–Th 'isochrons' with 10^4–10^5 year ages.

All of the continental arc rhyolitic rocks studied here have equilibrium or near-equilibrium $(^{238}U)/(^{230}Th)$, despite significant disequilibrium in associated intermediate rocks. In addition, two of the three rhyolites have Th isotopic compositions that differ significantly from those of associated intermediate rocks. These data imply that rhyolites generally have crustal residence times of 10^5 years or more, consistent with observations in some larger silicic systems (Davies *et al.*, 1994; Reid *et al.*, 1997). This does not require the rhyolites to have been entirely molten over this period. Instead, the crystal contents of these rhyolites could wax and wane depending on the fluxes of heat and volatiles through the systems over time (e.g. Mahood, 1990). However, periods of crystallization could not commonly be associated with significant fractionation of minerals with large and differing partition coefficients for U and Th (e.g. zircon and sphene).

The processes by which the rhyolitic magmas were generated appear to vary from site to site. Nearly pure Rayleigh fractionation appears to have generated rhyolites from intermediate predecessors at the Katmai–Novarupta volcanic system, whereas rhyolites at Medicine Lake require significant assimilation. Nevertheless, near-equilibrium $(^{238}U)/(^{230}Th)$ values for all of the rhyolitic rocks allow residence times for the rhyolitic magmas to be $> 10^5$ years, consistent with long-term warming of the crust from persistent mafic magmatism (e.g. Hildreth, 1981).

CONCLUSIONS

The lengths of time required for differentiating and storing magmas in the crust appear to significantly increase with increasing SiO_2 concentration. Basalts and basaltic andesites commonly have trace element and isotopic compositions, as well as ^{238}U–^{230}Th disequilibrium, that reflect the compositions of the parental basalts. Crustal residence times are commonly less than a few thousand years based on the presence of ^{226}Ra–^{230}Th disequilibrium noted in other arc basalts.

Andesites and dacites from the centers studied here are generated by AFC processes from basaltic parents. In most cases, the assimilants are relatively young plutons or crystal mushes, as indicated by the lack of variation in Sr and Nd isotopic compositions with changing SiO_2 concentrations. In other words, the assimilation is 'cryptic' in that it is invisible to many geochemical monitors of petrological processes. The magmatic compositions of these assimilants appear to have resulted from long periods of magmatism, which gradually replaced the older crust with younger mantle-derived materials (Kay *et al.*, 1990). Additional disequilibrium can be generated during the differentiation that generates andesites and dacites, as a result of partitioning of U and Th between assimilated melts and residual crystals.

The larger-volume rhyolites studied here (Crater Lake and Katmai–Novarupta) appear to have been generated by crystal fractionation of andesites and dacites with minor assimilation. In contrast, the genesis of the Glass Mountain rhyolite from Medicine Lake seems to have involved significant assimilation. The equilibrium or near-equilibrium $(^{238}U)/(^{230}Th)$ ratios for all of the rhyolites suggest that the rhyolites all had a protracted period of differentiation and accumulation. The rhyolite from Crater Lake accumulated, at least in part, over tens of thousands of years or more. The rhyolites from the Medicine Lake and Katmai–Novarupta clearly had a protracted time of differentiation ($>10^5$ years). Therefore, residence times for magmas in the continental crust increase by a minimum of 2–3 orders of magnitude with increasing SiO_2 concentrations from basalt to rhyolite.

ACKNOWLEDGEMENTS

Wes Hildreth, Julie Donnelly-Nolan, and Charlie Bacon are thanked for samples, unpublished data, encouragement, discussions over the years, and reviews of an early draft of the manuscript. Reviews by Wendy Bohrson, Shan de Silva, Olgeir Sigmarsson, and Chris Hawkesworth; editorial comments by Marjorie Wilson; and discussions with Jon Blundy, Simon Turner, and Rhiannon George significantly improved the manuscript. John Eichelberger is thanked for assistance in sample collection at the Katmai–Novarupta center. Terry Plank and Katherine Kelley are thanked for the exceptional major and trace element analyses. Yemane Asmerom helped develop the analytical techniques at Minnesota. Early alpha spectrometry analyses of Medicine Lake samples by Joe Hill launched this study. This work was funded by NSF grants EAR96-28486 (M.K.R.), EAR99-80605 (R.L.E.), and EAR00-01003(M.K.R., K.W.W.S.), as well as a University of Minnesota McKnight Land-Grant Fellowship to R.L.E.

REFERENCES

Asmerom, Y. & Edwards, R. L. (1995). U-series isotope evidence for the origin of continental basalts. *Earth and Planetary Science Letters* **134**, 1–7.

Bacon, C. R. (1983). Eruptive history of Mount Mazama and Crater Lake Caldera, Cascade Range, USA. In: Aramaki, S. & Kushiro, I. (eds) *International Symposium on Arc Volcanism, Tokyo–Hakone, Japan. Journal of Volcanology and Geothermal Research* **18**, 57–115.

Bacon, C. R. (1985). Implications of silicic vent patterns for the presence of large crustal magma chambers. *Journal of Geophysical Research B* **90**, 11243–11252.

Bacon, C. R. (1990). Calc-alkaline, shoshonitic, and primitive tholeiitic lavas from monogenetic volcanoes near Crater Lake, Oregon. *Journal of Petrology* **31**, 135–166.

Bacon, C. R. & Druitt, T. H. (1988). Compositional evolution of the zoned calcalkaline magma chamber of Mount Mazama, Crater Lake, Oregon. *Contributions to Mineralogy and Petrology* **98**, 224–256.

Bacon, C. R., Gunn, S. H., Lanphere, M. A. & Wooden, J. L. (1994). Multiple isotopic components in Quaternary volcanic rocks of the Cascade arc near Crater Lake, Oregon. *Journal of Petrology* **35**, 1521–1556.

Bacon, C. R., Persing, H. M., Wooden, J. L. & Ireland, T. R. (2000). Late Pleistocene granodiorite beneath Crater Lake Caldera, Oregon, dated by ion microprobe. *Geology* **28**, 467–470.

Baker, M. B., Grove, T. L., Kinzler, R. J., Donnelly-Nolan, J. M. & Wandless, G. A. (1991). Origin of compositional zonation (high-alumina basalt to basaltic andesite) in the Giant Crater Lava Field, Medicine Lake Volcano, northern California. *Journal of Geophysical Research B, Solid Earth and Planets* **96**, 21819–21842.

Beard, J. S. (1995). Experimental, geological, and geochemical constraints on the origins of low-K silicic magmas in oceanic arcs. In: Brown, M., Rushmer, T. & Sawyer, E. W. (eds) *Mechanisms and Consequences of Melt Segregation from Crustal Protoliths. Journal of Geophysical Research B* **100**, 15593–15600.

Beattie, P. (1993). The generation of uranium series disequilibria by partial melting of spinel peridotite; constraints from partitioning studies. *Earth and Planetary Science Letters* **117**, 379–391.

Bergantz, G. W. (1995). Changing techniques and paradigms for the evaluation of magmatic processes. *Journal of Geophysical Research B* **100**, 17603–17613.

Blundy, J. D. (1998). Heavy REE are compatible in clinopyroxene on the spinel lherzolite solidus. *Earth and Planetary Science Letters* **160**, 493–504.

Bohrson, W. A. & Spera, F. J. (2001). Energy-constrained open-system magmatic processes II: application of energy-constrained assimilation and fractional crystallization (EC-AFC) model to magmatic systems. *Journal of Petrology* **42**, 1019–1041.

Brophy, J. G., Dorais, M. J., Donnelly-Nolan, J. M. & Singer, B. S. (1996). Plagioclase zonation styles in hornblende gabbro inclusions from Little Glass Mountain, Medicine Lake Volcano, California; implications for fractionation mechanisms and the formation of composition gaps. *Contributions to Mineralogy and Petrology* **126**, 121–136.

Cameron, K. L. & Hanson, G. N. (1982). Rare earth element evidence concerning the origin of voluminous Mid-Tertiary rhyolitic ignimbrites and related volcanic rocks, Sierra Madre Occidental, Chihuahua, Mexico. *Geochimica et Cosmochimica Acta* **46**, 1489–1503.

Cheng, H., Edwards, R. L., Hoff, J., Gallup, C. D., Richards, D. A. & Asmerom, Y. (2000). The half-lives of uranium-234 and thorium-230. *Chemical Geology* **169**, 17–33.

Clark, S. K., Reagan, M. K. & Plank, T. (1998). Trace element and U-series systematics for 1963–1965 tephras from Irazu Volcano, Costa Rica; implications for magma generation processes and transit times. *Geochimica et Cosmochimica Acta* **62**, 2689–2699.

Condomines, M. & Sigmarsson, O. (1993). Why are so many arc magmas close to ^{238}U–^{230}Th radioactive equilibrium? *Geochimica et Cosmochimica Acta* **57**, 4491–4497.

Coombs, M. L. & Gardner, J. E. (2001). Shallow-storage conditions for the rhyolite of the 1912 eruption at Novarupta, Alaska. *Geology* **9**, 775–778.

Coombs, M. L., Eichelberger, J. C. & Rutherford, M. J. (2000). Magma storage and mixing conditions for the 1953–1974 eruptions of Southwest Trident Volcano, Katmai

National Park, Alaska. *Contributions to Mineralogy and Petrology* **140**, 99–118.

Davies, G. R., Halliday, A. N., Mahood, G. A. & Hall, C. M. (1994). Isotopic constraints on the production rates, crystallisation histories and residence times of pre-caldera silicic magmas, Long Valley, California. *Earth and Planetary Science Letters* **125**, 17–37.

Donnelly-Nolan, J. M. (1998). Abrupt shift in delta^{18}O values at Medicine Lake Volcano (California, USA). *Bulletin of Volcanology* **59**, 529–536.

Donnelly-Nolan, J. M., Champion, D. E., Miller, C. D., Grove, T. L. & Trimble, D. A. (1990). Post-11,000-year volcanism at Medicine Lake Volcano, Cascade Range, Northern California. *Journal of Geophysical Research B* **95**, 19693–19704.

Donnelly-Nolan, J. M., Champion, D. E., Grove, T. L., Baker, M. B., Taggart, J. E., Jr & Bruggman, P. E. (1991). The Giant Crater Lava Field: geology and geochemistry of a compositionally zoned, high-alumina basalt to basaltic andesite eruption at Medicine Lake Volcano, California. *Journal of Geophysical Research, B, Solid Earth and Planets* **96**, 21843–21863.

Druitt, T. H. & Bacon, C. R. (1989). Petrology of the zoned calcalkaline magma chamber of Mount Mazama, Crater Lake, Oregon. *Contributions to Mineralogy and Petrology* **101**, 245–259.

Edwards, R. L., Chen, J. H. & Wasserburg, G. J. (1987). ^{238}U–^{234}U–^{230}Th–^{232}Th systematics and the precise measurement of time over the past 500,000 years. *Earth and Planetary Science Letters* **81**, 175–192.

Eichelberger, J. C. (1981). Mechanism of magma mixing at Glass Mountain, Medicine Lake Highland Volcano, California. In: Johnston, D. A. & Donnelly-Nolan, J. M. (eds) *Guides to Some Volcanic Terranes in Washington, Idaho, Oregon, and Northern California. US Geological Survey Circular* **838**, 183–189.

Eichelberger, J. C., Chertkoff, D. G., Dreher, S. T. & Nye, C. J. (2000). Magmas in collision; rethinking chemical zonation in silicic magmas. *Geology* **28**, 603–606.

Eiler, J. M., Crawford, A. J., Elliott, T. R., Farley, K. A., Valley, J. W. & Stolper, E. M. (2000). Oxygen isotope geochemistry of oceanic-arc lavas. *Journal of Petrology* **41**, 229–256.

Elliott, T., Plank, T., Zindler, A., White, W. & Bourdon, B. (1997). Element transport from slab to volcanic front at the Mariana Arc. *Journal of Geophysical Research B* **102**, 14991–15019.

Gill, J. B. (1981). *Orogenic Andesites and Plate Tectonics*. Berlin: Springer, 390 pp.

Gill, J. B., Morris, J. D. & Johnson, R. W. (1993). Timescale for producing the geochemical signature of island arc magmas; U–Th–Po and Be–B systematics in Recent Papua New Guinea lavas. *Geochimica et Cosmochimica Acta* **57**, 4269–4283.

Goldstein, S. J., Murrell, M. T. & Janecky, D. R. (1989). Th and U isotopic systematics of basalts from the Juan de Fuca and Gorda Ridges by mass spectrometry. *Earth and Planetary Science Letters* **96**, 134–146.

Graham, I. J., Cole, J. W., Briggs, R. M., Gamble, J. A. & Smith, I. E. M. (1995). Petrology and petrogenesis of volcanic rocks from the Taupo Volcanic Zone; a review. In: Simmons, S. F. & Weaver, S. D. (eds) *Taupo Volcanic Zone, New Zealand. Journal of Volcanology and Geothermal Research* **68**, 59–87.

Grove, T. L. & Donnelly-Nolan, J. M. (1986). The evolution of young silicic lavas at Medicine Lake Volcano, California; implications for the origin of compositional gaps in calc-alkaline series lavas. *Contributions to Mineralogy and Petrology* **92**, 281–302.

Grove, T. L., Gerlach, D. C. & Sando, T. W. (1982). Origin of calc-alkaline series lavas at Medicine Lake Volcano by fractionation, assimilation and mixing. *Contributions to Mineralogy and Petrology* **80**, 160–182.

Grove, T. L., Kinzler, R. J., Baker, M. B., Donnelly-Nolan, J. M. & Lesher, C. E. (1988). Assimilation of granite by basaltic magma at Burnt Lava Flow, Medicine Lake Volcano, Northern California; decoupling of heat and mass transfer. *Contributions to Mineralogy and Petrology* **99**, 320–343.

Grove, T. L., Donnelly-Nolan, J. M. & Housh, T. B. (1997). Magmatic processes that generated the rhyolite of Glass Mountain, Medicine Lake Volcano, N. California. *Contributions to Mineralogy and Petrology* **127**, 205–223.

Halliday, A. N., Fallick, A. E., Dickin, A. P., Mackenzie A. B., Stephens, W. E. & Hildreth, W. (1983). The isotopic and chemical evolution of Mount St. Helens. *Earth and Planetary Science Letters* **63**, 241–256.

Hardee, H. C. & Larson, D. W. (1977). Viscous dissipation effects in magma conduits. *Journal of Volcanology and Geothermal Research* **2**, 113–144.

Hart, S. R. (1984). A large-scale isotope anomaly in the Southern Hemisphere mantle. *Nature* **309**, 753–757.

Hawkesworth, C. J., Blake, S., Evans, P., Hughes, R., Macdonald, R., Thomas, L. E., Turner, S. & Zellmer, G. (2000). Time scales of crystal fractionation in magma chambers—integrating physical, isotopic and geochemical perspectives. *Journal of Petrology* **41**, 991–1006.

Heiken, G. (1978). Plinian-type eruptions in the Medicine Lake Highland, California, and the nature of the underlying magma. *Journal of Volcanology and Geothermal Research* **4**, 375–402.

Herrstrom, E. A., Reagan, M. K. & Morris, J. D. (1995). Variations in lava composition associated with flow of asthenosphere beneath southern Central America. *Geology* **23**, 617–620.

Hickey-Vargas, R., Lopez-Escobar, L., Moreno-Roa, H., Reagan, M. K., Morris, J. D. & Wyan, J. G. (2002). Multiple subduction components in the mantle wedge: evidence from eruptive centers in the Central Southern Volcanic Zone, Chile. *Geology* **30**, 199–202.

Hildreth, W. (1981). Gradients in silicic magma chambers: implications for lithospheric magmatism. *Journal of Geophysical Research B* **86**, 10152–10192.

Hildreth, W. (1983). The compositionally zoned eruption of 1912 in the Valley of Ten Thousand Smokes, Katmai National Park, Alaska. In: Aramaki, S. & Kushiro, I. (eds) *International Symposium on Arc Volcanism, Tokyo–Hakone, Japan. Journal of Volcanology and Geothermal Research* **18**, 1–56.

Hildreth, W. (1987). New perspectives on the eruption of 1912 in the Valley of Ten Thousand Smokes, Katmai National Park, Alaska. *Bulletin of Volcanology* **49**, 680–693.

Hildreth, W. & Fierstein, J. (2000). Katmai volcanic cluster and the great eruption 1912. *Geological Society of America Bulletin* **112**, 1594–1620.

Hirschmann, M., M., Asimow, P. D., Ghiorso, M. S. & Stolper, E. M. (1999). Calculation of peridotite partial melting from thermodynamic models of minerals and metals; III, controls on isobaric melt production and the effect of water on melt production. *Journal of Petrology* **40**, 831–851.

Hopson, C. & Mattinson, J. (1990). Chelan Migmatite Complex; a Cretaceous protodiapiric mash zone in the North Cascades, Washington. *Geological Society of America, Abstracts with Programs* **22**, 29–30.

Huppert, H. E. & Sparks, R. S. J. (1988). The generation of granitic magmas by intrusion of basalt into continental crust. *Journal of Petrology* **29**, 599–624.

Kay, S. M., Kay, R. W., Citron, G. P. & Perfit, M. R. (1990). Calc-alkaline plutonism in the intra-oceanic Aleutian Arc, Alaska. In: Kay, S. M. & Rapela, C. W. (eds) *Plutonism from Antarctica to Alaska. Geological Society of America, Special Paper* **241**, 233–255.

Kelley, K. A., Plank, T., Ludden, J. & Staudigel, H. (2003). The composition of altered oceanic crust at ODP Sites 801 and 1149. *Geochemistry, Geophysics, Geosystems* (in press).

Kinzler, R. J., Donnelly-Nolan, J. M. & Grove, T. L. (2000). Late Holocene hydrous mafic magmatism at the Paint Pot Crater and Callahan Flows, Medicine Lake Volcano, N. California and the influence of H_2O in the generation of silicic magmas. *Contributions to Mineralogy and Petrology* **138**, 1–16.

Landwehr, D., Blundy, J., Chamorro-Perez, E. M., Hill, E. & Wood, B. (2001). U-series disequilibria generated by partial melting of spinel lherzolite. *Earth and Planetary Science Letters* **188**, 329–348.

LaTourrette, T. Z., Kennedy, A. K. & Wasserburg, G. J. (1993). Thorium–uranium fractionation by garnet; evidence for a deep source and rapid rise of oceanic basalts. *Science* **261**, 739–742.

Layne, G. D. & Sims, K. W. (2000). Secondary ion mass spectrometry for the measurement of $^{232}Th/^{230}Th$ in young volcanic rocks. *Journal of Mass Spectrometry* **203**, 187–198.

Lowenstern, J. B., Persing, H. M., Wooden, J. L., Lanphere, M., Donnelly-Nolan, J. & Grove, T. L. (2000). U–Th dating of single zircons from young granitoid xenoliths; new tools for understanding volcanic processes. *Earth and Planetary Science Letters* **183**, 291–302.

Mahood, G. A. (1990). Reply to Comment of R. S. J. Sparks, H. E. Huppert, and C. J. N. Wilson on 'Evidence for long residence times of rhyolitic magma in the Long Valley magmatic system: the isotopic record in precaldera lavas of Glass Mountain'. *Earth and Planetary Science Letters* **99**, 395–399.

Mertzman, S. A., Jr (1977). The petrology and geochemistry of the Medicine Lake Volcano, California. *Contributions to Mineralogy and Petrology* **62**, 221–247.

Mertzman, S. A., Jr (1979). Strontium isotope geochemistry of a low potassium olivine tholeiite and two basalt–pyroxene andesite magma series from the Medicine Lake Highland, California. *Contributions to Mineralogy and Petrology* **70**, 81–88.

Mertzman, S. A., Jr & Williams, R. J. (1981). Genesis of Recent silicic magmatism in the Medicine Lake Highland, California; evidence from cognate inclusions found at Little Glass Mountain. *Geochimica et Cosmochimica Acta* **45**, 1463–1478.

Plank, T. & Langmuir, C. H. (1998). The chemical composition of subducting sediment and its consequences for the crust and mantle. *Chemical Geology* **145**, 325–394.

Reagan, M. K. & Gill, J. B. (1989). Coexisting calcalkaline and high-niobium basalts from Turrialba Volcano, Costa Rica; implications for residual titanates in arc magma sources. *Journal of Geophysical Research, B* **94**, 4619–4633.

Reagan, M. K., Morris, J. D., Herrstrom, E. A. & Murrell, M. T. (1994). Uranium series and beryllium isotope evidence for an extended history of subduction modification of the mantle below Nicaragua. *Geochimica et Cosmochimica Acta* **58**, 4199–4212.

Reid, M. R., Coath, C. D., Harrison, T. M. & McKeegan, K. D. (1997). Prolonged residence times for the youngest rhyolites associated with Long Valley Caldera; ^{230}Th–^{238}U ion microprobe dating of young zircons. *Earth and Planetary Science Letters* **150**, 27–39.

Sigmarsson, O., Condomines, M., Morris, J. D. & Harmon, R. S. (1990). Uranium and ^{10}Be enrichments by fluids in Andean arc magmas. *Nature* **346**, 163–165.

Sigmarsson, O., Martin, H. & Knowles, J. (1998). Melting of a subducting oceanic crust from U–Th disequilibria in Austral Andean lavas. *Nature* **394**, 566–569.

Sigmarsson, O., Chmeleff, J., Morris, J. & Lopez-Escobar, L. (2002). Origin of ^{226}Ra–^{230}Th disequilibria in arc lavas from southern Chile and magma transfer time. *Earth and Planetary Science Letters* **196**, 189–196.

Sisson, T. W. & Grove, T. L. (1993). H_2O in basalt and basaltic andesite glass inclusions from four subduction-related volcanoes. *Earth and Planetary Science Letters* **117**, 619–635.

Sisson, T. W., Grove, T. L. & Anonymous (1990). Water-saturated melting of calc-alkaline high alumina basalt and basaltic andesite. *EOS Transactions, American Geophysical Union* **71**, 648.

Smith, D. R. & Leeman, W. P. (1987). Petrogenesis of Mount St. Helens dacitic magmas. *Journal of Geophysical Research B* **92**, 10313–10334.

Smith, R., J. (1979). Ash-flow magmatism. In: Chapin, C. E. & Elston, W. E. (eds) *Ash-Flow Tuffs. Geological Society of America, Special Paper* **180**, 5–28.

Spera, F. J. & Bohrson, W. A. (2001). Energy-constrained open-system magmatic processes I: general model and energy-constrained assimilation and fractional crystallization (EC-AFC) formulation. *Journal of Petrology* **42**, 999–1018.

Stolper, E. M. & Newman, S. (1994). The role of water in the petrogenesis of Mariana Trough magmas. *Earth and Planetary Science Letters* **121**, 293–325.

Sun, S. S. & McDonough, W. F. (1989). Chemical and isotopic systematics of oceanic basalts; implications for mantle composition and processes. In: Saunders, A. D. & Norry, M. J. (eds) *Magmatism in the Ocean Basins. Geological Society, London, Special Publications* **42**, 313–345.

Tanton, L. T. E., Grove, T. L. & Donnelly-Nolan, J. (2001). Hot, shallow mantle melting under the Cascades volcanic arc. *Geology* **29**, 631–634.

Thomas, R. B., Hirschmann, M. M., Cheng, H., Reagan, M. K. & Ewards, R. L. (2002). $(^{231}Pa/^{235}U)$–$(^{230}Th/^{238}U)$ of young volcanic rocks from Nicaragua and Costa Rica and the influence of flux melting on U-series systematics of arc lavas. *Geochimica et Cosmochimica Acta* **66**, 4287–4309.

Thompson, A. B. & Connolly, J. A. D. (1995). Melting of the continental crust; some thermal and petrological constraints on anatexis in continental collision zones and other tectonic settings. In: Brown, M., Rushmer, T. & Sawyer, E. W. (eds) *Mechanisms and Consequences of Melt Segregation from Crustal Protoliths. Journal of Geophysical Research B* **100**, 15565–15579.

Todt, W., Cliff, R. A., Hanser, A. & Hofmann, A. W. (1996). Evaluation of a ^{202}Pb–^{205}Pb double spike for high precision lead isotope analysis. In: Hart, S. R. & Basu, A. (eds) *Earth Processes: Reading the Isotope Code. Geophysical Monograph, American Geophysical Union* **95**, 429–437.

Turner, S., Blundy, J., Wood, B. & Hole, M. (2000*a*). Large ^{230}Th-excesses in basalts produced by partial melting of spinel peridotite. *Chemical Geology* **162**, 127–136.

Turner, S., Bourdon, B., Hawkesworth, C. & Evans, P. (2000*b*). ^{226}Ra–^{230}Th evidence for multiple dehydration events, rapid melt ascent and the time scales of differentiation beneath the Tonga–Kermadec island arc. *Earth and Planetary Science Letters* **179**, 581–593.

Turner, S., Evans, P. & Hawkesworth, C. J. (2001). Ultrafast source-to-surface movement of melt at island arcs from ^{226}Ra–^{230}Th systematics. *Science* **292**, 1363–1366.

Volpe, A. M. (1992). ^{238}U–^{230}Th–^{226}Ra disequilibrium in young Mt. Shasta andesites and dacites. *Journal of Volcanology and Geothermal Research* **53**, 227–238.

Volpe, A. M. & Hammond, P. E. (1991). ^{238}U–^{230}Th–^{226}Ra disequilibria in young Mount St. Helens rocks; time constraint for magma fractionation and crystallization. *Earth and Planetary Science Letters* **107**, 475–486.

Wood, B. J., Blundy, J. D. & Robinson, J. A. C. (1999). The role of clinopyroxene in generating U-series disequilibrium during mantle melting. *Geochimica et Cosmochimica Acta* **63**, 1613–1620.

Zellmer, G., Turner, S. & Hawkesworth, C. (2000). Timescales of destructive plate margin magmatism; new insights from Santorini, Aegean volcanic arc. *Earth and Planetary Science Letters* **174**, 265–281.

Zucca, J. J., Fuis, G. S., Milkereit, B., Mooney, W. D. & Catchings, R. D. (1986). Crustal structure of northeastern California. *Journal of Geophysical Research B* **91**, 7359–7382.